CHARACTERIZING SUBSURFACE HYDRAULIC CHARACTERISTICS AT ZHUOSHUI RIVER ALLUVIAL FAN, TAIWAN

by

Yu-Li Wang

_____

A Thesis Submitted to the Faculty of the

DEPARTMENT OF HYDROLOGY AND WATER RESOURCES

In Partial Fulfillment of the Requirements

For the Degree of

MASTER OF SCIENCE
WITH A MAJOR IN HYDROLOGY

In the Graduate College

THE UNIVERSITY OF ARIZONA

2016

STATEMENT BY AUTHOR

The thesis has been submitted in partial fulfillment of requirements for a master's degree at the University of Arizona and is deposited in the University Library to be made available to borrowers under rules of the Library.

Brief quotations from this thesis are allowable without special permission, provided that an accurate acknowledgement of the source is made. Requests for permission for extended quotation from or reproduction of this manuscript in whole or in part may be granted by the head of the major department or the Dean of the Graduate College when in his or her judgment the proposed use of the material is in the interests of scholarship.   In all other instances, however, permission must be obtained from the author.

SIGNED: <u>Yu-Li Wang</u>

APPROVAL BY THESIS DIRECTOR

This thesis has been approved on the date shown below:

<u>05/10/2016</u>

Tian-Chyi Jim Yeh   Date

Professor of Hydrology and Water Resources

<u>Acknowledge</u>

Table of Contents

List of Figures

Abstract

The objective of this study is to estimate 2-D spatial distribution of hydraulic conductivity (Ks) of Zhuoshui River alluvial fan, Taiwan, using groundwater level data from 88 wells and stream stage data from 4 gauging stations. In order to accomplish this analysis, wavelet analysis is first carried out to investigate the periodic cycles of groundwater level, precipitation, and stream stage. The results of the analysis show that variations of groundwater level and stream stage are highly correlated in terms of seasonal and annual periods. Subsequently, seasonal variations of groundwater level in response to stream stage variation are utilized to estimate the Ks spatial distribution by spatiotemporal cross correlation analysis, cokriging, and river stage tomography. Prior to applications of these methods to the alluvial fan, performances of each approach are evaluated and compared with reference field of a noise free synthetic experiment. It is found that all of the approaches could yield similar general spatial pattern of Ks. Nevertheless, river stage tomography seems to reveal a higher resolution of spatial Ks distribution. When the geologic zones are provided in river stage tomography analysis as prior information, the accuracy of estimated Ks values improves. Finally, results of the applications to data of the alluvial fan reveal that the apex and southeast of the alluvial fan are regions with relative high Ks and the Ks values gradually decrease toward the shoreline of the fan. These two areas are considered as the possible main recharge regions of the aquifer. It is also observed that Ks at northern alluvial fan is slightly larger than that at southern. These findings seem consistent with the geologic evolution of this alluvial fan.

1. Introduction

For the purpose of managing groundwater resources in a basin, information about hydraulic property distributions, which controls water and contaminant movement and distributions in the basin, is required. With this information, numerical surface water and groundwater models can be used for long-term management of water resources through estimation, prediction, and scenario analysis of surface water and groundwater systems.

Cross correlation analysis is a useful tool to study and evaluate the correlation or sensitivity between two variables. Dagan [1982], Kitanidis and Vomvoris [1983], Hoeksema and Kitanidis [1984], Kitanidis [1995], Yeh et al. [1995, 1996], and others employed the cross correlation between observed heads and spatial heterogeneity of hydraulic properties to estimate spatial distributed hydraulic parameters in confined aquifers. Sun et al. (2013) studied the represented range of estimated hydraulic properties in spatial domain from early, intermediate, and late time data respectively by cross correlation analysis. Mao et al. (2013) studied the sensitivity of observed head with respect to unsaturated parameters in response to a pumping event at a synthetic unconfined aquifer.

Hydraulic tomography (HT) is a technique of characterizing subsurface heterogeneity. The original idea of HT is jointly interpreting the information carried by drawdown fields triggered from multiple pumping tests. HT is conducted by cross correlation between measurements, such as observed head or flux, and spatial heterogeneity of hydraulic properties and has been applied successively to small-scale synthetic aquifers, laboratory sandboxes, plot-scale fields, and a fractured granite field site [Yeh and Liu, 2000; Vesselinov et al., 2001; Liu et al., 2002; Zhu and Yeh, 2005, 2006; Bohling et al., 2007; Illman et al., 2007, 2009; Li et al., 2007a; Liu et al., 2007; Straface et al., 2007; Hao et al., 2008; Zha et al. 2015; Tso et al., 2015].

Unlike the relative small scale fields whose groundwater flow field could be fluctuated by controlled anthropogenic activities such as pumping easily, it is difficult or may cost a lot to produce significant groundwater fluctuation with relative high signal-noise ratio under kilometers even basin scale fields. Therefore, utilizing stimuli provided by nature becomes the potential option to study the subsurface characteristics. Natural stimuli such as atmospheric pressure variations at the surface, periodic solid earth tides, ocean tides, precipitation at the surface, and even earthquake are found to induce groundwater fluctuation from a few centimeters to meters with spatial scales ranging from local to regional flow systems [DeWiest, 1965; Rojstaczer, 1988; Rojstaczer and Riley, 1990; Hsieh et al., 1988; Davis et al., 2000; Lin et al., 2004; Li et al., 2007b]. Likewise, recharge from and discharge to surface water bodies such as rivers and lakes induce hydraulic gradients over the different

spatial scales, too [Duffy et al., 1978; Nevulis et al., 1989; Sophocleous, 1991; Barlow et al., 2000; Vazquez-Sune et al., 2007].

River stage tomography is a concept of extracting subsurface heterogeneity information from stream induced groundwater level variation. The time scale of variations could be event, seasonal, or even annual based. Yeh et al. [2009] revealed the possibility of characterizing basin scale subsurface heterogeneity by fusing the information carried with the river induced groundwater level perturbation. The experiment carried out in a synthetic stream-aquifer system demonstrated the potential of river stage tomography utilizing event based flood waves.

While the performance of HT has been evaluated by numerical, sandbox experiments and some recent field applications, its ability for high-resolution aquifer characterization under basin scale remains to have more assessed. Especially, the benefits of HT have not been demonstrated and evaluated in comparison with other approaches under synthetic conditions in basin scale. As a result, the objective of this paper is to quantitatively evaluate three approaches for estimating Ks fields using groundwater level perturbation induced by stream stage variation in a synthetic aquifer whose geometry is similar to the interest alluvial fan. The synthetic aquifer represents the ideal situation where true hydraulic property fields, boundary conditions, head measurements, as well as stream gauges are exactly known and noise free. These two approaches to be evaluated include (1) the cross-correlation approach and (2) river stage tomography approach. The robustness' of estimated Ks fields from the three approaches are appraised by comparing with the reference field.

Thus, in the first part of this study, we analyze the hydrographs collected at the study site for the preparation of mapping the hydraulic heterogeneity. We then conduct a synthetic alluvial fan resembling the field site around Zhuoshui River, Taiwan. Using measurements of stream perturbed groundwater hydraulic head, we compare and discuss the results of Ks estimation between different approaches and scenarios. Finally, the estimated Ks spatial distribution at the study alluvial fan using field data is discussed.

2. Study Site
2.1. Water Environment and Challenge in Taiwan

Taiwan is a 36000 km^2 island, about half of South Carolina State. Two third of it land area is neither mountain nor hill range. The elevation varies from 4000 m to sea level in only 70 km distance. It takes only eight hours for the flood wave propagate from mountain range into the ocean. Although the annual precipitation is about 2500 mm/year which is approximately 2.5 times the world average, the mean annual available water per capita in Taiwan is 4074 m^3, only one fifth of the world average. Due to the limitation of steep terrain, Taiwan encounters crisis of not only too much but also too less water.

Another factor that causes such small amount of available water per person is because of the highly temporal and spatial non-uniform rainfall in Taiwan. If define May till October belong to wet season and the else are dry season, the wet and dry seasonal precipitation ratio at northern Taiwan is 6:4, while at middle and southern is 8:2 and 9:1 respectively. The huge seasonality rainfall variation enforces the stress on the reservoir operation satisfying the water demand during the half-year long dry season.

Maintaining reservoir storage capacity is a critical issue as well. The reservoirs in Taiwan have only 1.9 billion tons of effective water storage capacity in total while the annual water supply from the reservoirs is 4.3 billion tons (i.e. one fourth of the total annual water demand.). However, because Taiwan is a relatively young island in geology aspect, soil is relatively easier to be eroded. The accumulation of mud from mountain during heavily rainfall event such as typhoon leads to the reduction of reservoir water supply capability. In average, 30% of the storage capacity has been occupied.

Water is a kind of necessary resources for the living of human and other life in the Earth. It is not only the basis of development of society but also will affect the social economic structure and migration of natural environment. Therefore, water resource is one of the key factors that maintain the sustainable human society. To countries such as Taiwan, where not worry about poverty, but rather about the uneven distribution, the groundwater management is a relative important option to provide the stable water supply.

2.2. Site Description

It was suggested that using river stage variations for characterizing groundwater basins requires sensor networks that provide long-term and spatially distributed monitoring of excitations, as well as response signals on the land surface and in the subsurface (Yeh et al. 2009). Therefore, application of river stage tomography in real

world situations would require a groundwater basin that has been well-instrumented and monitored, including a large number of observation wells at different locations with screens opened at different depths and a sufficient number of river gauging stations. Most importantly, long term and high frequency (at least hourly) records of groundwater levels, river stage, precipitation, and other hydro-meteorological processes over the basin are required to complete this analysis. Few basins in the world meet this requirement because of costs associated with the operations and maintenances. The Zhuoshui River alluvial fan in Taiwan is uniquely qualified for this purpose because a massive amount of hydro-geological data has been collected since 1992 primarily for the purpose of irrigation groundwater management and earthquake investigations.

The Zhuoshui River alluvial fan is located at middle Taiwan. It is about 70 km long and 40 km width and with an area of 1800 km^2. The Zhuoshui River flows from east to west from the central mountainous area through the alluvial fan before discharging into Taiwan Strait. The Central Geological Survey [1994, 1999] constructed 12 hydro-geological profiles for the alluvial fan based on the core samples from drilled wells. An unconfined and three confined aquifers named layer 1 to layer 4 were approximately identified from shallow to 300 meters depth. Based on the prior geological investigation, all of the aquifers are connected to each other at apex of the fan. This alluvial fan consists of several layers of Holocene to Pleistocene sands and gravels that formed the three confined aquifers separated by marine mud [Central Geological Survey, 1994, 1999]. It is suggested that the rising and falling of the mean sea levels caused by global climate change late in the Quaternary Period formed the layered structure of the alluvial fan [cite Water Resources Agency, 2014]. Massive gravels, which comprise many layers of the upper fan, tend to pinch out toward the west of the fan till shoreline, while the mud layers thicken. An interface between the gravels and the arenaceous sediments was identified to separate the partially confined and confined aquifers.

The alluvial fan is bounded by 1 km width Wu River at the north and 400 meters width Beigang River at the south. Furthermore, 2 km width Zhuoshui River penetrates through the mountain pass between Bagua Plateau and Douliu Hill at the center of the fan from east to west. Besides, the alluvial fan is also bounded by 300 m height Bagua Plateau and 400 m height Douliu Hill at its northeast and southeast respectively. The elevation of the fan is about 100 m at the apex and 0 m at the tail. The elevation suddenly drops from 100 to 30 m within 10 km after leaving the mountain pass between Bagua Plateau and Douliu Hill. Groundwater could be observed 30 m below the ground surface at the upper fan and 10 m below the ground at middle and tail.

2.3. Data Collection

A Groundwater Monitoring Network System was gradually established throughout the fan since 1992 and was expanded to the current size at 1997. The network consists of 70 evenly distributed hydrological stations, where a total of 188 monitoring wells are installed at various depths ranging from 24 through 306 m. Most of the wells are screened at only single depth, and the water levels at all of the wells have been recorded hourly since 1997. There are 21 stream gauges installed at rivers through the fan. Stream stage or flow rate utilized in this study are labeled in figure 1b. There are four stream gauging stations along the Zhuoshui River located at the apex, middle, and the tail of the alluvial fan named Zhangyun Bridge, Xizhou Bridge, Ziqiang Bridge, and Xibin Bridge, respectively. Stream gauge (Dadu Bridge) at downstream of Wu River at northern boundary of the alluvial is used as well. River stage and flow rate have hourly records as well. In addition, hourly meteorological data has been collected from about 50 weather stations since 2009. We select Xiashuipu weather station located at apex of the fan for the precipitation analysis. Daily precipitation records since 1997 are borrowed from Chiayi weather station which locates 40 km southern from the Zhuoshui River.
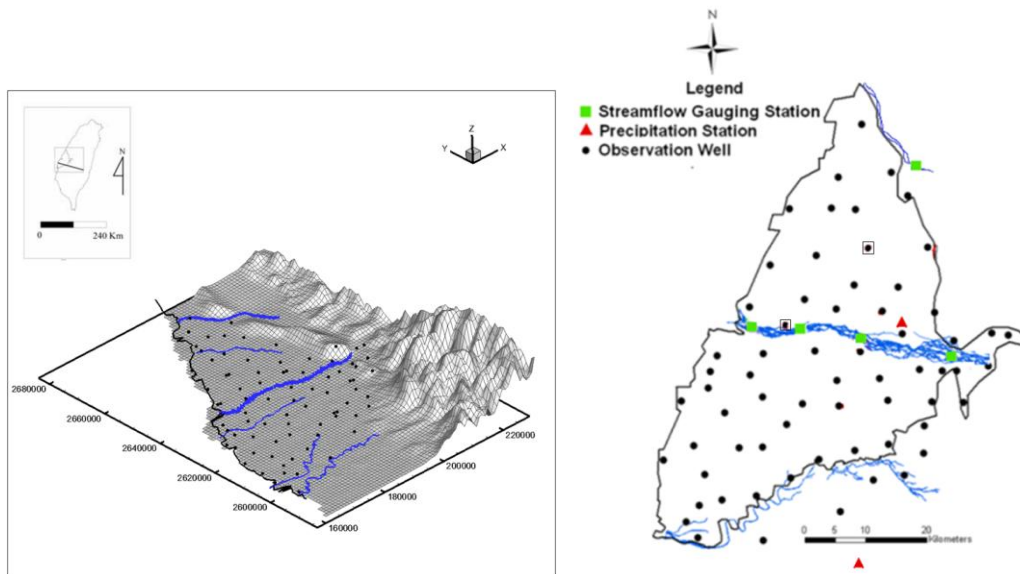
Figure 1. a) Topographic map and b) distributions of wells, precipitation stations, and stream gauges in the Zhuoshui River fan. Only stations utilized in this study are labeled. The green rectangles represent the river gauge station. The gauging stations along Zhuoshui River from upper to downstream are Zhangyun Bridge, Xizhou Bridge, Ziqiang Bridge, and Xibin Bridge, respectively. The red triangle located at apex of the fan is Xiashuipu while located below the scale is Chiayi precipitation station. The black circles with square are the groundwater monitoring wells 1 and 15 km away from the river named Tan-Cian (1-1) and Si-Hu (1), respectively.

3. Numerical Experiment Setup

3.1. River-Aquifer System

Following the geometry of Zhuoshui River alluvial fan, a horizontal 80*60 square elements domain is built. Each element is 1.0 km* 1.0 km. The western and eastern boundaries are constant head boundaries representing coast and headwater respectively. The headwater is 120 m higher than the coast. Head gradient between headwater and coast is used to mimic the natural regional subsurface flow gradient in Zhuoshui River alluvial fan. 50 km long Zhuoshui River penetrates through the middle of the fan while the Wu river is at the north. They are represented by blue line as illustrated in figure 2. Both of the rivers are treated as time varying prescribed head boundaries. The rest of the boundaries are no flow boundary because they are either hills that could be considered as watersheds between two different basins or relative small streams that has little effect on the groundwater fluctuation. The Zhuoshui River, monitoring wells, and stream gauges are set based on their real coordinate. Figure 2 shows the cell layout of the modeling domain and the relative locations for the river, the flow boundaries, and observation wells.

3.2. Sedimentation Profile

The reference sedimentation profile we used here contains gravel, sand, and clay. The spatial hydraulic conductivity distribution of the profile is estimated by the joint interpretation of electrical resistivity and well logs [cite Tsai]. Values and spatial distribution of Ks for all the elements in the synthetic aquifer are shown in figures 3. The spatial Ks distribution is generated by the following statistical characteristics: Mean of Ks for gravel, sand, and clay are 3.6, 0.036, and 0.00036 (m/hr). The variances of ln(Ks) are 0.3, 1.0, and 2.2. The correlation scales are 10, 25, and 40 km for both x and y directions, respectively. Mean of Ss for gravel, sand, and clay are 0.05, 0.0005, and 0.000005 (1/m) while variances are zero.

The sedimentation profile follows gravel, sand, and clay from the apex to the tail of the alluvial fan respectively. The pattern agrees with the sedimentation process of the river that angular conglomerates and breccias tend to settle down at the headwater whose transportation energy is relatively higher, while the arkose and finer materials such as silt and clay tend to be at the middle and tail of the river that has lower transportation energy. Due to the drift of the flow path of Zhuoshui River between the old flow path (now Old Zhuoshui River) and the current one before the levees build, the sedimentation profile at northern part of middle alluvial fan appears to have sand and silt/clay interlocked with each other. It seems that the southern part of the alluvial fan does not have such significant subsurface heterogeneity compared with the northern part. It is probably that instead of Zhuoshui River, the sediment is

transported by Beigang River and the source of the sediment is from Douliu Hill. The gravel region located at the northern boundary could probably be attributed to the alluvium of another 1.0 km with river, Wu River. [Water Resources Agency, 2014]
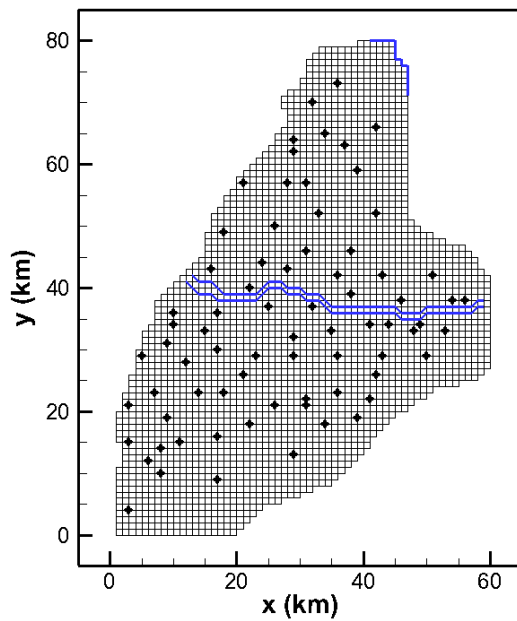
Figure 2. Plan view of the synthetic groundwater basin showing geometry of the river and the aquifer. Dark circles represent the observation wells, and blue lines represent stream boundary while the rest represents constant head or no flow boundaries.
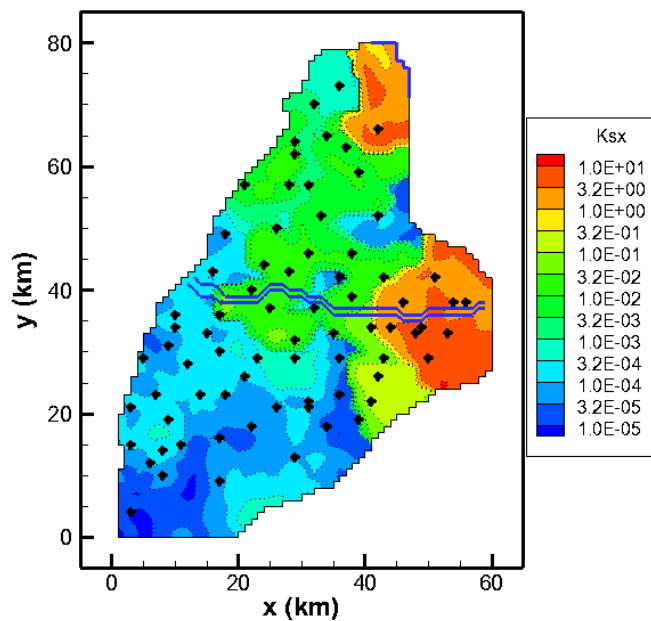
Figure 3. Reference hydraulic conductivity Ks (m/hr) field. Colors represent spatial distributions of gravel (red), sand (green), and clay (blue) in the synthetic domain. Dark circles represent locations of the observation wells, and blue lines represent

stream boundary while the rest represents constant head boundaries.

4. Essential Approaches

Spatial-temporal cross-correlation analysis, cokriging, and river stage tomography are carried out to analyze the groundwater level variation in response to stream stage change. Information carried by the observed head is extracted and utilized to estimate the hydraulic property spatial distribution.

Three scenarios are considered in the third approach to examine the importance of prior information of subsurface (i.e. prior ensemble mean Ks) to the estimated field. The ensemble mean is a stochastic concept. It describes the mean value at given location of the realizations while realization is a possible spatial or temporal distribution of variable with given spatial or temporal mean and variance. In other word, ensemble mean is the average over imaginary domain while spatial mean is the average over spatial domain and temporal mean is the average over time domain (figure 4). Under ergodicity condition, ensemble mean will equal to spatial as well as temporal mean.
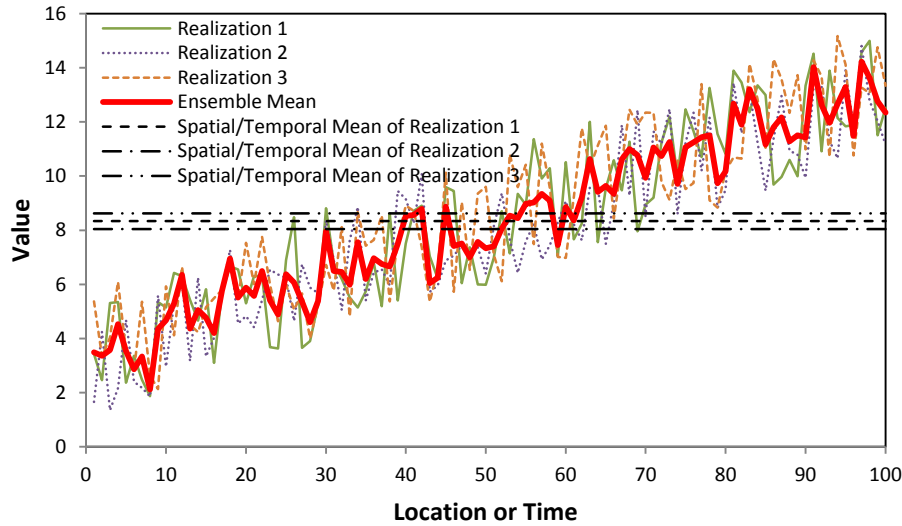
Figure 4. Schematic diagram of realization (thin lines), ensemble mean (bold red line), and spatial or temporal mean (horizontal lines).

In geostatistical inversion, the model usually starts from uniform ensemble mean before it is conditioned by observed data. This scenario represents the situation that we have no any knowledge about the geologic structure of the site. With the given ensemble mean value as the initial Ks field, the model evaluates and estimates the parameter perturbations above the mean (scenario 1).

In scenario 2, we start the river stage tomography from zonation ensemble mean (i.e. different ensemble mean value for different zone.) by assuming we already know the exactly boundary between zones. This represents our prior knowledge about the zonation or distribution of reference Ks field.

Since the second scenario is just an ideal case and is not realistic at all because usually we don't have boundary information between zones, the third scenario is introduced. The scenario 3 starts from zonation ensemble mean as well; however, the difference is we don't exactly know where the boundaries of zones are. That is, we guess the potential boundaries from the estimate Ks field of scenario 1, then assign the different ensemble mean value to each zones and estimate the ensemble mean Ks field again. Some zones may have ensemble mean value closer to their true ensemble mean hopefully, while some may have terribly initial guess. This scenario represents the more general situation that the information provided by well logs or geophysical surveys can reveal some structures in the aquifer, which could be served as the prior knowledge about the site.

4.1. Approache 1: Cross-Correlation Analysis

Correlation between river stage and groundwater fluctuation is investigated by cross correlation analysis. The cross correlation is an index providing the similarity of two time series as a function of time lag of one relative to the other. The geo-statistical definition of cross-correlation is

$$Cor(L) = \frac{\frac{1}{N-L}\sum_{i=1}^{N-L}[(h_1(i)-\overline{h_1})(h_2(i+L)-\overline{h_2})]}{\sqrt{\frac{1}{N}\sum_{i=1}^{N}(h_1(i)-\overline{h_1})^2}\sqrt{\frac{1}{N}\sum_{i=1}^{N}(h_2(i)-\overline{h_2})^2}}$$

This formula illustrates the cross correlation $Cor(L)$ between two time series $h_1(i)$ and $h_2(i+L)$ with the identical data length where i is time, L is time lag, and N is number of data in single signal. The value of time lag L should be between $\pm N$. $\overline{h_1}$ and $\overline{h_2}$ represent the average of the entire signal without considering time lag.

The possible value of cross correlation should be between 1 and -1 if sufficient temporal length of data is provided. The positive cross correlation represents the two signals are positive correlated at certain time lag while the negative represents the two signals are negative correlated with respect to the certain lag of time. If the cross correlation is 1, it suggests that the two signals are perfect correlated.

In this study, h_1 and h_2 represent time series of stream stage and groundwater level, respectively. The positive time delay represents that the river stage rises earlier and reaches its pick before the groundwater level does while the negative time delay means the groundwater responses earlier than the river stage (figure 5).

Maximum cross correlation of each station are selected and extrapolated through the entire alluvial fan using three dimensional ordinary kriging. It is expected that nearby regions will have similar maximum cross correlation value and lag of time if they are employed by similar subsurface hydraulic properties.
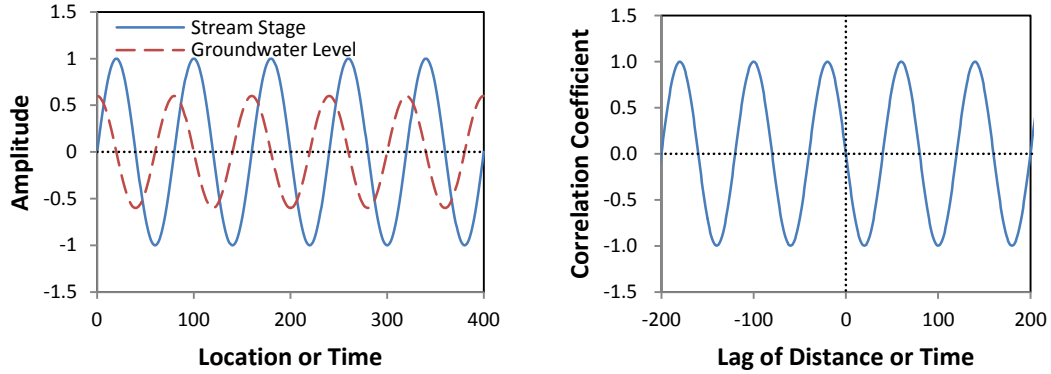
Figure 5. Schematic diagram of cross correlation. a) Stream stage (sine) and groundwater level (cosine) series. Both of the signals have period equal to 80. b) Associated cross correlation functions. In this case, if the groundwater level perturbation is induced by stream stage perturbation, the time lag will be 60. However, if the river is a gaining stream (?), lag of time will be 20.

4.2. Approache 2: Cokriging
4.2.1. Kriging

Kriging is a linear unbiased spatial interpolation and extrapolation contour algorithm which considers the prior knowledge of spatial statistic structure such as correlation function and correlation scale. These prior knowledges are important. For instance, in a perfectly stratified geologic formation, the sampled attribute at a point in a layer is expected to be highly correlated with that at any location within the same layer. Since kriging weights are derived based on the spatial correlation structure, the contribution of the sample thus will be weighted heavily for the estimate at any point in the same layer in spite of the distances between the sample and estimate. However, one must recognize that the correlation structure implies the most likely spatial relationship. As a result, kriging yields the best linear unbiased estimate in statistical sense only. More detailed discussion about kriging could be found at book named Flow through Heterogeneous Geologic Media by Yeh et al. (2015).

4.2.2. Simple Kriging

Assume $Z^*(x_i)$ is a spatial stationary process with constant sample mean

$$E[Z^*(x_i)] = \overline{Z^*}(x_i)$$

where x_i is spatial location.

$Z(x_i)$ is perturbation of $Z^*(x_i)$ above the mean, that is

$$Z(x_i) = Z^*(x_i) - \overline{Z^*(x_i)}$$

$Z(x_i)$ is the estimated value and is linear combination of $Z(x_i)$

$$Z(x_i) = \sum_{j=1}^{N} \lambda_j Z(x_j)$$

where λ_j is weighting and N is number of sampling point.

The optimal estimator requires that the error between the estimation and real value be minimal. Here we use mean square error as the object function.

$$object = E[[Z(x_i) - Z(x_i)]^2] = \frac{1}{N} \sum_{i=1}^{N} [Z(x_i) - Z(x_i)]^2$$

Substitute $Z(x_i)$ with $\sum_{j=1}^{N} \lambda_j Z(x_j)$ and yield

$$object = E[[[\sum_{j=1}^{N} \lambda_j Z(x_j)] - Z(x_i)]^2]$$

$$= E[\sum_{j=1}^{N} \lambda_j Z(x_j) \sum_{k=1}^{N} \lambda_k Z(x_k)] - E[\sum_{j=1}^{N} \lambda_j Z(x_j) Z(x_i)] - E[\sum_{k=1}^{N} \lambda_k Z(x_k) Z(x_i)] + E[Z(x_i) Z(x_i)]$$

$$= \sum_{j=1}^{N} \sum_{k=1}^{N} \lambda_j \lambda_k E[Z(x_j) Z(x_k)] - \sum_{j=1}^{N} \lambda_j E[Z(x_i) Z(x_j)] - \sum_{k=1}^{N} \lambda_k E[Z(x_i) Z(x_k)] + E[Z(x_i) Z(x_i)]$$

Since

$$E[Z(x_i) Z(x_j)] = Cov(x_i, x_j)$$

Thus,

$$object$$

$$= \sum_{j=1}^{N} \sum_{k=1}^{N} \lambda_j \lambda_k E[Z(x_j) Z(x_k)] - \sum_{j=1}^{N} \lambda_j E[Z(x_i) Z(x_j)] - \sum_{k=1}^{N} \lambda_k E[Z(x_i) Z(x_k)] + E[Z(x_i) Z(x_i)]$$

$$= \sum_{j=1}^{N} \sum_{k=1}^{N} \lambda_j \lambda_k Cov(x_j, x_k) - \sum_{j=1}^{N} \lambda_j Cov(x_i, x_j) - \sum_{k=1}^{N} \lambda_k Cov(x_i, x_k) + Cov(x_i, x_i)$$

Take $\dfrac{\partial}{\partial \lambda_j} = 0$ to minimize the object function

$$\frac{\partial object}{\partial \lambda_j} = \sum_{k=1}^{N} \lambda_k Cov(x_j, x_k) - Cov(x_i, x_j) = 0$$

$$\sum_{k=1}^{N} \lambda_k Cov(x_j, x_k) = Cov(x_i, x_j)$$

where $Cov(x_j, x_k)$ represents spatial covariance or variogram between sampling points which describes the degree of spatial dependence of a spatial random field or stochastic process, while $Cov(x_i, x_j)$ represents spatial covariance or variogram between sampling points and estimated location

Assume uniform spatial variance $Var(x)$. Divide both sides by $Var(x)$ leads to

$$\sum_{k=1}^{N} \lambda_k Cor(x_j, x_k) = Cor(x_i, x_j)$$

where $Cor(x_j, x_k)$ represents spatial correlation between sampling points while

$Cor(x_i, x_j)$ represents spatial correlation between sampling points and estimated location.

4.2.3. Ordinary Kriging

Assume sample mean equals to population mean

$$E[Z^*(x_j)] = E[Z_m^*(x_i)]$$

To satisfy the definition of unbiased estimator, the estimated mean should identical with population mean.

$$E[Z^*(x_i)] = E[Z_m^*(x_i)]$$

while $Z(x_i)$ is perturbation of $Z^*(x_i)$ above the mean, that is

$$Z(x_i) = Z^*(x_i) - \overline{Z^*}(x_i)$$

If we chose the linear estimator as our estimate,

$$Z(x_i) = \sum_{j=1}^{N} \lambda_j Z(x_j)$$

the linear estimator must satisfy the following condition

$$E[\sum_{j=1}^{N} \lambda_j Z(x_j)] = E[Z(x_j)]$$

Then we have

$$\sum_{j=1}^{N} \lambda_j = 1$$

Introduce this new criterion into simple kriging using Lagrange multiplier μ.

$$\sum_{k=1}^{N} \lambda_k Cor(x_j, x_k) + \mu = Cor(x_i, x_j) + 1$$

Express in matrix form leads to

$$\begin{bmatrix} Cor(x_j, x_k) & 1 \\ 1 & 0 \end{bmatrix} \begin{bmatrix} \lambda_k \\ \mu \end{bmatrix} = \begin{bmatrix} Cor(x_i, x_j) \\ 1 \end{bmatrix}$$

Adding the mean value back, the estimated spatial distribution will be

$$Z^*(x_i) = \sum_{j=1}^{N} \lambda_j Z^*(x_j)$$

whose conditional covariance or residual covariance function that evaluates the uncertainty of the estimated property at given location will be

$$res.Cov(x_i, x_{ii}) = Cov(x_i, x_{ii}) - \sum_{j=1}^{N} \lambda_j Cov(x_j, x_i)$$

where $Cov(x_i, x_{ii})$ represents prior covariance or prior spatial dependence between

estimated locations while $Cov(x_j, x_i)$ is covariance or spatial dependence between

sampling point and estimated location.

The uncertainty at locations with measurement will be zero,

$$Var(x_j) = 0$$

by assuming there aren't any measurement error been introduced. That is, the estimated value at sampling point will be identical with the measurement.

Here, we use exponential based variogram to describe the spatial dependence of stochastic process

$$Cov(x_i, x_j) = 1 - \exp\{-3[(\frac{dx}{csx})^2 + (\frac{dy}{csy})^2 + (\frac{dz}{csz})^2]^{0.5}\}$$

where dx, dy, and dz are distances with unit in [L] between two points in x, y, and z directions respectively. csx, csy, and csz are spatial correlation scales with unit in [L] in x, y, and z directions.

4.2.4. Cokriging

With given unconditional mean and spatial covariance functions of the hydraulic properties, cokriging is used to estimate the conditional expected value of the property conditioned on hard data (measurement hydraulic properties) and the observed head. The detailed of cokriging linear estimator is discuss in section 4.3.2.

In this study, we assume that there's no any hard data measurement. The cokriging linear estimator thus reduces to

$$\hat{f}^{(1)}(\mathbf{x}_0) = \mu_{j0}[h^*(\mathbf{x}_j) - h_e(\mathbf{x}_j)]$$

Since covariance of head and head, R_{hh}, is obtained by first order approximation governed by sensitivity of head with respect to hydraulic property, J_{hf}, and spatial correlation or covariance of hydraulic property, R_{ff}. Because J_{hf} is obtained by adjoint method which already includes the stream stage information from upper to downstream during solving the groundwater flow governing equation, we could treat cokriging as a technique considering correlation between point and line. Therefore, it is expected that the estimated spatial distribution of hydraulic property from cokriging could yield better spatial resolution compared with that from cross correlation analysis at regions where have relative high spatial variance or shorter correlation length.

4.3. Approache 3: River Stage Tomography

River stage tomography is a stochastic inverse method extended from hydraulic tomography. Instead of using drawdown data from different pumping tests, river stage tomography utilizes the groundwater variation in response to the river stage change to employ the property characterization.

The aim of this tomography technique is to estimate hydraulic properties of aquifers through the incorporation of nonlinear relationship between the system parameter (i.e., hydraulic conductivity, specific storage, etc.) and the system response (i.e., head, flux, etc.) during the estimation process by using a linear estimator iteratively. In other word, residual variances (estimate uncertainty) of estimated property at each element are considered.

It is expected that river stage tomography could utilize the usefulness of a given data set of a system response at a given time and location better in comparison with other two approaches (i.e. cross correlation and cokriging).

Below is a brief description of the linear estimator and associated iterative processes. Detailed discussion could be found at Yeh and colleagues' publications (Yeh et al., 1996, 2002, 2006; Zhang and Yeh, 1997; Hughson and Yeh, 2000; Yeh and Liu, 2000; Zhu and Yeh, 2005; Yeh and Zhu, 2007).

4.3.1. Simultaneous Successive Linear Estimator

A simultaneous successive linear stochastic estimator (SimSLE) is utilized to

include all groundwater level variation data from different stream stage variation during a river stage tomography survey simultaneously to estimate hydraulic properties of aquifers (Xiang et al., 2009). SimSLE is an extension based on successive linear estimator (SLE) developed by Yeh and colleagues. The procedures of simSLE is as following.

4.3.2. Cokriging and Associated Conditional Covariance

Suppose we discretize the study domain into N elements and we have collected o measurement and m observed head. With given unconditional mean and spatial covariance functions of the hydraulic properties (prior joint probability distribution, implicitly Gaussian), the SimSLE starts with cokriging (a stochastic linear estimator) to estimate the conditional expected value of the K conditioned on measured f^* (1×o) at $\mathbf{x}_i$ and the observed head at specific location $\mathbf{x}_j$ and time during specific seasonal stream stage variation, denoted by h^* (1×m). The cokriging linear estimator is,

$$\hat{f}^{(1)}(\mathbf{x}_0) = \lambda_{i0} f^*(\mathbf{x}_i) + \mu_{j0}[h^*(\mathbf{x}_j) - h_e(\mathbf{x}_j)] \quad [2]$$

where $\hat{f}^{(1)}(\mathbf{x}_0)$ is the cokriged f value at location $\mathbf{x}_0$ at the first iteration. It is an N×N matrix. h_e (m×1) is the simulated head at the observed location and time perturbed by the seasonal stream stage variation. The simulated head are obtained based on the field which could be an equivalent homogeneous medium, stratifying medium, or even heterogeneous medium.

The cokriging weight λ_{i0} (o×1) represents contribution of measurement perturbation f^* at i^{th} location to the estimate at location, $\mathbf{x}_0$. The contribution to the estimation from the observed head is denoted by μ_{j0} (m×1). These weights are obtained by solving the following system of equations:

$$\begin{bmatrix} R_{ff} & R_{fh} \\ R_{hf} & \varepsilon_{hh} \end{bmatrix} \begin{bmatrix} \lambda_{i0} \\ \mu_{j0} \end{bmatrix} = \begin{bmatrix} \varepsilon_{ff} \\ \varepsilon_{hf} \end{bmatrix} \quad [3]$$

Our prior knowledge of the spatial structure (the unconditional covariance function) of f is given by covariance between measurements R_{ff} (o×o). R_{hf} (m×o) is the unconditional cross covariance of f and h, which is determined by the first order approximation with the given R_{ff}. The unconditional covariance of h

ε_{hh} (m×m) is obtained by the first order approximation as well. That is,

$$R_{hf} = J_{hf} R_{ff} \qquad \varepsilon_{hf} = J_{hf} \varepsilon_{ff}$$
$$R_{fh} = R_{hf}{}^{T} \quad \text{and} \quad \varepsilon_{hh} = \varepsilon_{hf} J_{hf}{}^{T} \qquad [4]$$

where ε_{ff} (o×1) is covariance between measurements and unknown f at location

$\mathbf{x}_0$. ε_{hf} (m×1) is covariance between head and unknown f at location $\mathbf{x}_0$. J_{hf}

(m×o) is the sensitivity of head with respect to the change of parameter. The sensitivity matrix is evaluated using the adjoint state approach (Li and Yeh, 1998; Li and Yeh, 1999; Lu et al., 2015).

After obtaining the new estimate for all the elements using cokriging, the conditional covariance of f, $\varepsilon_{ff}^{(1)}$, is then determined by

$$\varepsilon_{ff}^{(1)} = R_{ff} - \lambda_{i0} R_{ff} - \mu_{j0} R_{hf} \quad [5]$$

The conditional covariance reflects the effect of data on the reduction of uncertainty in the estimated parameter field. Subsequently, the estimated K fields are used to solve groundwater flow equation with boundary and initial conditions for the conditional effective head fields, $h^{(1)}$.

4.3.3. Kriging Like Update

Following cokriging, a linear estimator of the following form,

$$\hat{f}^{(r+1)}(\mathbf{x}_0) = \hat{f}^{(r)}(\mathbf{x}_0) + \omega^{(r)}[h^* - h^{(r)}] \quad [6]$$

is used to improve the estimate for iteration $r > 1$, where $\omega^{(r)}$ is the weight term, representing the contribution of the difference between the observed and simulated conditional heads (i.e., h^* and $h^{(r)}$, respectively). The weights are determined by solving the following kriging like equation:

$$\omega^{(r)}(\varepsilon_{hh}^{(r)} + \Theta^{(r)}\delta) = \varepsilon_{hf}^{(r)} \quad [7]$$

The terms $\varepsilon_{hh}^{(r)}$ and $\varepsilon_{fh}^{(r)}$ are the conditional covariance and the conditional cross covariance at iteration (r), which are evaluated using the first order approximation (i.e. equations (4)) using the conditional covariance of f (i.e., $\varepsilon_{ff}^{(r)}$ which is obtained from equation (5) for the first iteration).

26

A dynamic stabilizer, $\Theta^{(r)}$, is added to the diagonal elements of $\varepsilon_{hh}^{(r)}$ (δ is Dirac delta function) to stabilize the solution. This technique is also known as Levenberg-Marquardt Algorithm or damped least-squares, which interpolates between the Gauss–Newton algorithm and the gradient descent to solve non-linear least squares problems. The dynamic stabilizer at iteration, r, is the maximum value of the diagonal elements of $\varepsilon_{hh}^{(r)}$ at that iteration times a user-specified multiplier (see Yeh et al., 1996).

4.3.4. Residual Covariance Update

After completion of the estimation using kriging like update for all elements in the domain, the conditional covariance of f is updated subsequently by

$$\varepsilon_{ff}^{(r+1)} = \varepsilon_{ff}^{(r)} - \omega \varepsilon_{hf}^{(r)} \quad [8]$$

4.3.5. Convergence Criteria

The iteration steps of SimSLE are the same as those in the SLE algorithm used in Yeh et al. (1996). For noise-free hydrographs, the convergence is achieved if 1) change in variances that represent spatial variability of the estimated hydraulic properties between current and last iterations is smaller than a specified tolerance (i.e., the spatial variance of the estimates stabilizes), implying that the SimSLE cannot improve the estimation any further; 2) change of simulated heads between successive iterations is smaller than the tolerance, indicating that the estimates will not significantly improve the head field. If one of the two criteria is met, the estimates are considered to be optimal and the iterations are terminated.

Measurements and Initial Guess

Forward Simulation

Cokriging

SLE

Convergence Criteria

Figure 6a. Flow chart of simSLE.

$\hat{h}$ Observed head.

$\hat{f} = \ln(\hat{K}) - \ln(\overline{K}^{(0)})$ Measurement perturbation.

$f^{(0)} = \ln(K^{(0)}) - \ln(\overline{K}^{(0)})$ Initial ensemble mean field.

$\varepsilon_{ff}^{(0)}$ Initial variance (estimated uncertainty).

$h^{(0)} = G(K^{(0)})$ Groundwater flow forward simulation.

J_{hf} Solve sensitivity by adjoint approach for the

preparation of forming covariance matrix.

$\varepsilon_{hf} = J_{hf}\varepsilon_{ff}^{(0)}$

$\varepsilon_{hh} = J_{hf}\varepsilon_{ff}^{(0)}J_{hf}^{T}$ Form covariance matrix by first order approximation

$R_{hf} = J_{hf}R_{ff}$

for the preparation of cokriging.

$R_{ff}\mu + R_{hf}\lambda = \varepsilon_{ff}$

$R_{hf}\mu + \varepsilon_{hh}\lambda = \varepsilon_{hf}$ Do cokriging and update estimated field by the

$f^{(1)} = f^{(0)} + \mu\hat{f} + \lambda(\hat{h} - h^{(0)})$

measurements.

$\varepsilon_{ff}^{(1)} = \varepsilon_{ff}^{(0)} - \mu\varepsilon_{ff} - \lambda\varepsilon_{hf}$ Calculate residual covariance.

i = 1

$h^{(i)} = G(K^{(i)})$ Groundwater flow forward simulation. J_{hf} Solve sensitivity by adjoint approach for the preparation of forming covariance matrix. $\varepsilon_{hf} = J_{hf}\varepsilon_{ff}^{(i)}$ $\varepsilon_{hh} = J_{hf}\varepsilon_{ff}^{(i)}J_{hf}^{T}$ Form covariance matrix by first order approximation for the preparation of cokriging like update. $\varepsilon_{hh}\lambda = \varepsilon_{hf}$ $f^{(i+1)} = f^{(i)} + \lambda(\hat{h} - h^{(i)})$ Do cokriging like update. $\varepsilon_{ff}^{(i+1)} = \varepsilon_{ff}^{(i)} - \lambda\varepsilon_{hf}$ Calculate residual covariance.

$i = i + 1$

Converge and Stop

Figure 6b. Flow chart of simSLE.

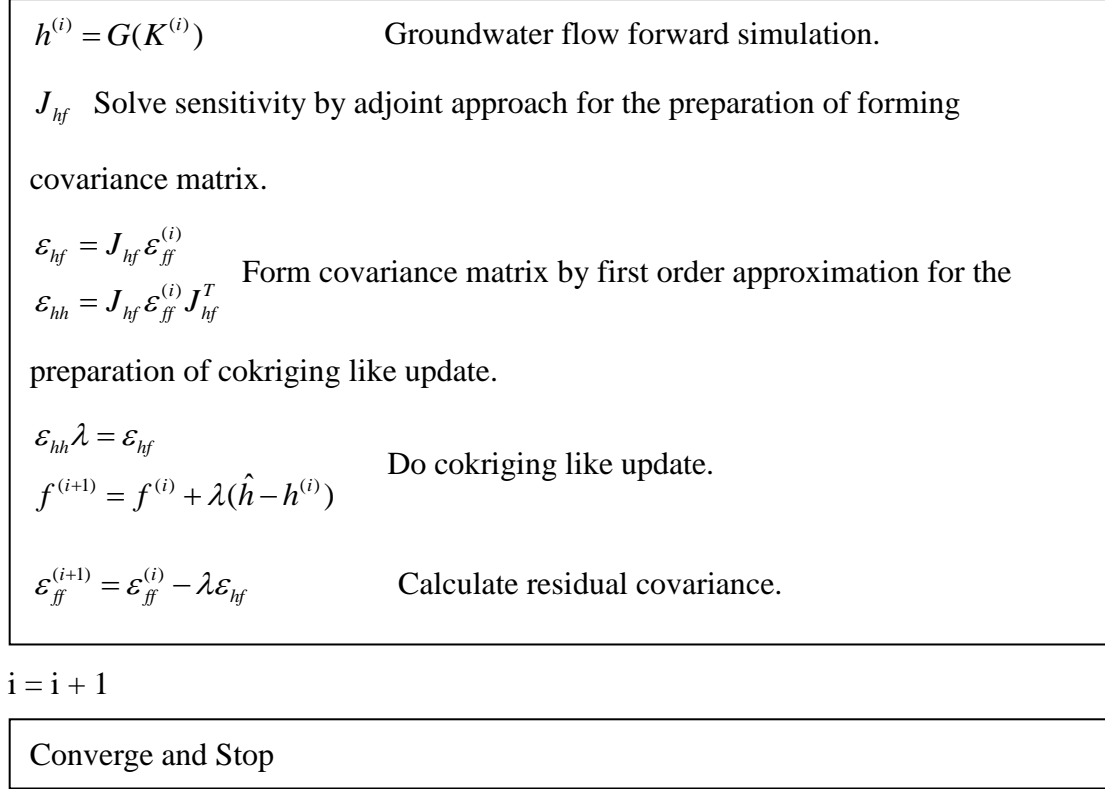## 4.4. Sensitivity
4.4.1. Sensitivity Equation Method

The transient state groundwater flow in variably saturated media could be described by

$$\nabla[K(h)\nabla(h+z)] = [\varepsilon S_s + C(h)]\frac{\partial h}{\partial t} + Q \quad [1.1]$$

$$h + z = H$$

where K is hydraulic conductivity [L/T], h is pressure head [L], z is elevation head [L], S_s is specific storage [1/L], $C = \dfrac{d\theta(h)}{dh}$ is moisture release capacity [1/L], t is time [T], Q is source and sink term [1/T], and ε is a transitioning parameter, that is

$$\varepsilon = \begin{cases} 1, \ h \ge 0 \\ 0, otherwise \end{cases}$$

with initial condition

$$H(\mathbf{x},0) = \hat{H}(\mathbf{x},0) \quad [1.2]$$

and boundary conditions

$$H(\Gamma_1) = \hat{H}(\mathbf{x},t) \ \text{ on } \ \Gamma_1 \ \text{ and } \ -K\nabla H \cdot \mathbf{n} = \hat{q} \ \text{ on } \ \Gamma_2 \quad [1.3]$$

Take partial deviation of [1.1] with respect to α_k yields the sensitivity equation

$$\nabla \cdot [\frac{DK(h)}{D\alpha_k} \nabla(h+z)] + \nabla \cdot [K(h)\nabla\phi] = \frac{D[\varepsilon S_s + C(h)]}{D\alpha_k}\frac{\partial h}{\partial t} + [\varepsilon S_s + C(h)]\frac{\partial \phi}{\partial t} + \frac{\partial Q}{\partial \alpha_k}$$

$$\nabla \cdot [\frac{\partial K(h)}{\partial \alpha_k}\nabla(h+z) + \frac{\partial K(h)}{\partial h}\phi\nabla(h+z)] + \nabla \cdot [K(h)\nabla\phi]$$

$$= \frac{\partial [\varepsilon S_s + C(h)]}{\partial \alpha_k}\frac{\partial h}{\partial t} + \frac{\partial [\varepsilon S_s + C(h)]}{\partial h}\phi\frac{\partial h}{\partial t} + [\varepsilon S_s + C(h)]\frac{\partial \phi}{\partial t} + \frac{\partial Q}{\partial \alpha_k} \qquad [2.1]$$

where the state sensitivity, $\phi(\mathbf{x},t)$, represents the sensitivity of the hydraulic head to a change of the property, α_k, at a given location.

$$\phi = \frac{\partial h}{\partial \alpha_k}$$

$$\alpha_k = \left[K, S_s, Q, \hat{H}, \hat{q}, \alpha, n \right]$$

while k = 1, …N, which is the total number of parameters.

Because $K(h)$ and $C(h)$ are multivariable function which is expressed as a function of saturated hydraulic conductivity K_s, pressure h, and other empirical parameters, such as α for an exponential model, or α and n for Van Genugten-Muller model. Thus, we need to use total derivative to describe their variation with respect to each variables.

Assume variables in α_k are independent with each other. (i.e. $\frac{\partial K}{\partial S_s} = 0$, $\frac{\partial K}{\partial \alpha} = 0$, and etc.)

$$\frac{DK}{D\alpha_k} = \frac{\partial K}{\partial \alpha_k} + \frac{\partial K}{\partial h}\frac{dh}{d\alpha_k} + \frac{\partial K}{\partial S_s}\frac{dS_s}{d\alpha_k} = \frac{\partial K}{\partial \alpha_k} + \frac{\partial K}{\partial h}\frac{dh}{d\alpha_k}$$

The associated initial condition is

$$\phi(\mathbf{x},0) = \frac{\partial \hat{H}(\mathbf{x},0)}{\partial \alpha_k} = 0 \quad [2.2]$$

and boundary conditions are

$$\phi(\mathbf{x},t) = \frac{\partial \hat{H}(\mathbf{x},t)}{\partial \alpha_k}\Big|_{\Gamma_1} = 0 \quad \text{on} \quad \Gamma_1 \quad [2.3]$$

and

$$-[\frac{\partial K}{\partial \alpha_k}\nabla H + K\nabla\phi] \cdot n_j = \frac{\partial \hat{q}}{\partial \alpha_k} = 0 \quad \text{on} \quad \Gamma_2 \quad [2.4]$$

Equation 2.1 is linear equation since K(h) and C(h) is independent with ϕ, thus,

sensitivity equation method will be computational efficient than perturbation method. However, one still need to solve the forward model for N+1 times.

To solve the sensitivity equation with the boundary and initial conditions, the head fields, $H(\mathbf{x},t)$, should be obtained first by solving the flow equation with given K and S_s fields as well as Q($\mathbf{x}$).

4.4.2. Adjoint Method

Since sensitivity equation is still computational cost if there are lots of parameters to be determined, we need to choose another method to calculate sensitivity. The adjoint method is a better option because the number of forward model to be solved is only based on the number of observation. In reality, it is usually that the number of observation is much less than that of parameters.

The brief derivation of adoint method is as following.

The observed data $O(\alpha_k, H)$ at specific location x_0 and time t_0 could be described as

$$O\delta(x-x_0, t-t_0)$$

$$= G$$

$$= \int_T \int_\Omega G d\Omega dT$$

where T is time domain and Ω is spatial domain.

Because G is a multi-variable function, the sensitivity of G with respect to the property, α_k, will be

$$\frac{DG}{D\alpha_k} = \int_T \int_\Omega \left(\frac{\partial G}{\partial \alpha_k} + \frac{\partial G}{\partial h}\frac{\partial h}{\partial \alpha_k}\right) d\Omega dT$$

$$= \int_T \int_\Omega \left(\frac{\partial G}{\partial \alpha_k} + \frac{\partial G}{\partial h}\phi\right) d\Omega dT \quad [3]$$

To eliminate the contribution of ϕ, which is computational cost to be solved, the adjoint variable λ is introduced.

Start form the sensitivity equation [2.1]. Multiplying with an arbitrary adjoint variable λ and integrating them over time T and domain Ω gives

$$\int_T \int_\Omega \lambda \{ \nabla \cdot [\frac{\partial K(h)}{\partial \alpha_k} \nabla(h+z) + \frac{\partial K(h)}{\partial h} \phi \nabla(h+z)]$$

$$+\nabla \cdot [K(h)\nabla\phi]$$

$$-\frac{\partial[\varepsilon S_s + C(h)]}{\partial \alpha_k}\frac{\partial h}{\partial t} - \frac{\partial[\varepsilon S_s + C(h)]}{\partial h}\phi\frac{\partial h}{\partial t} \qquad \text{[4.1] [4.2] [4.3] [4.4] [4.5]}$$

$$-[\varepsilon S_s + C(h)]\frac{\partial \phi}{\partial t}$$

$$-\frac{\partial Q}{\partial \alpha_k}\}d\Omega dT$$

Equation (4) Term (4.1)

Let λ be a twice continuously differentiable variable satisfying the requirement of Green's identities that relates the bulk with the boundary of a region on which differential operators act. Using Green's first identity,

$$\int_V (a\nabla b + b\nabla a)dV = \int_A abdA$$

[4.1] becomes

$$\int_T [\int_\Gamma \lambda \frac{\partial K(h)}{\partial \alpha_k}\nabla(h+z)d\Gamma - \int_\Omega \frac{\partial K(h)}{\partial \alpha_k}\nabla\lambda\nabla(h+z)d\Omega$$

$$+\int_\Gamma \lambda\phi\frac{\partial K(h)}{\partial h}\nabla(h+z)d\Gamma - \int_\Omega \phi\frac{\partial K(h)}{\partial h}\nabla\lambda\nabla(h+z)d\Omega]dT \qquad \text{[4.1.1]}$$

Equation (4) Term (4.2)

Using Green's second identity

$$\int_v [a\nabla(b\nabla c) - c\nabla(b\nabla a)]dv = \int_A b(a\nabla c - c\nabla a)dA$$

Term (4.2) becomes

$$\int_T \{\int_\Omega \phi\nabla\cdot[K(h)\nabla\lambda]d\Omega - \int_\Gamma \phi K(h)\nabla\lambda d\Gamma + \int_\Gamma \lambda K(h)\nabla\phi d\Gamma\}dt \quad \text{[4.2.1]}$$

Equation (4) Term (4.4)

Use integration by part

$$\int_\Omega \int_T [\varepsilon S_s + C(h)]\lambda \frac{\partial \phi}{\partial t}dtd\Omega$$

$$= \int_\Omega \{[\varepsilon S_s + C(h)]\phi\lambda \Big|_{t=0}^{t=final} - \int_T \frac{\partial[\varepsilon S_s + C(h)]\lambda}{\partial t}\phi dt\}d\Omega$$

$$= \int_\Omega \{[\varepsilon S_s + C(h)]\phi\lambda \Big|_{t=0}^{t=final} - \int_T \varepsilon S_s \frac{\partial\lambda}{\partial t}\phi dt - \int_T \frac{\partial C(h)\lambda}{\partial t}\phi dt\}d\Omega$$

$$= \int_{\Omega} ([\varepsilon S_s + C(h)]\phi\lambda\big|_{t=0}^{t=final} - \int_T \frac{\partial C(h)}{\partial t}\lambda\phi dt - \int_T (\varepsilon S_s + C(h))\frac{\partial \lambda}{\partial t}\phi dt)d\Omega$$

Here, we separate $\dfrac{\partial \phi}{\partial t}$ into initial and final time step for the later usage.

Substituting (4.1.1), (4.2.1), (4.3), (4.4.1), and (4.5) into (4) gives the adjoint integration term which equals to zero

$$\int_T \{-\int_\Omega \phi\frac{\partial K(h)}{\partial h}\nabla\lambda\nabla(h+z)d\Omega - \int_\Omega \frac{\partial K(h)}{\partial \alpha_k}\nabla\lambda\nabla(h+z)d\Omega + \int_\Omega \phi\nabla\cdot[K(h)\nabla\lambda]d\Omega$$

$$-\int_\Omega \frac{\partial[\varepsilon S_s + C(h)]}{\partial \alpha_k}\frac{\partial h}{\partial t}\lambda d\Omega + \int_\Omega [\varepsilon S_s + C(h)]\frac{\partial \lambda}{\partial t}\phi d\Omega - \int_\Omega \lambda\frac{\partial Q}{\partial \alpha_k}d\Omega\}dT$$

$$+\int_T\{\int_\Gamma \lambda K(h)\nabla\phi d\Gamma - \int_\Gamma \phi K(h)\nabla\lambda d\Gamma + \int_\Gamma \lambda\frac{\partial K(h)}{\partial \alpha_k}\nabla(h+z)d\Gamma + \int_\Gamma \lambda\phi\frac{\partial K(h)}{\partial h}\nabla(h+z)d\Gamma\}dT$$

$$-\int_\Omega [\varepsilon S_s + C(h)]\phi\lambda\big|_{t=0}^{t=final}d\Omega = 0$$

[5]

Substituting adjoint integration term [5] into marginal sensitivity of performance function [3] and rearranging them

$$\frac{DG}{D\alpha_k}$$

$$= \int_T\int_\Omega (\frac{\partial G}{\partial \alpha_k} + \frac{\partial G}{\partial h}\phi)d\Omega dT + \text{adjoint integration term}$$

$$= \int_T\int_\Omega \{\frac{\partial G}{\partial \alpha_k} + \phi[\frac{\partial G}{\partial h} + \nabla\cdot[K(h)\nabla\lambda] + [\varepsilon S_s + C(h)]\frac{\partial \lambda}{\partial t} - \frac{\partial K(h)}{\partial h}\nabla\lambda\nabla(h+z)]\}d\Omega dt$$

$$+\int_T\int_\Omega \{-\frac{\partial K(h)}{\partial \alpha_k}\nabla\lambda\nabla(h+z) - \frac{\partial[\varepsilon S_s + C(h)]}{\partial \alpha_k}\frac{\partial h}{\partial t}\lambda - \frac{\partial Q}{\partial \alpha_k}\lambda\}d\Omega dt$$

$$+\int_T (\int_\Gamma \lambda K(h)\nabla\phi d\Gamma - \int_\Gamma \phi K(h)\nabla\lambda d\Gamma + \int_\Gamma \lambda\frac{\partial K(h)}{\partial \alpha_k}\nabla(h+z)d\Gamma + \int_\Gamma \lambda\phi\frac{\partial K(h)}{\partial h}\nabla(h+z)d\Gamma)dt$$

$$-\int_\Omega [\varepsilon S_s + C(h)]\phi\lambda\big|_{t=0}^{t=final}d\Omega$$

[6]

Applying the initial and boundary conditions that the sensitivity of the hydraulic head to a change of the property α_k is zero at prescribed head boundary and the sensitivity of the hydraulic flux to a change of the property α_k is zero at prescribed flux boundary

$$\phi(\mathbf{x},t) = \frac{\partial \hat{H}(\mathbf{x},t)}{\partial \alpha_k}\Big|_{\Gamma_1} = 0 \quad \text{on} \quad \Gamma_1 \quad [2.3]$$

33

$$-[\frac{\partial K}{\partial \alpha_k}\nabla H + K\nabla\phi]\cdot n_j = \frac{\partial \hat{q}}{\partial \alpha_k} = 0 \quad \text{on} \quad \Gamma_2 \quad [2.4]$$

Set adjoint variable λ field satisfying the following adjoint equation

$$\frac{\partial G}{\partial h} + \nabla\cdot[K(h)\nabla\lambda] + [\varepsilon S_s + C(h)]\frac{\partial\lambda}{\partial t} - \frac{\partial K(h)}{\partial h}\nabla\lambda\nabla(h+z)$$

$$= \nabla\cdot[K(h)\nabla\lambda] + [\varepsilon S_s + C(h)]\frac{\partial\lambda}{\partial t} - \frac{\partial K(h)}{\partial h}\nabla\lambda\nabla(h+z) + \frac{\partial G}{\partial h}$$

$$= \text{diffusion term} + \text{storage change term} + \text{advection term} + \text{source/sink term}$$

$$= 0$$

When solving the equation, we set $t' = t_{final} - t$ and then the adjoint equation is transformed with the expression of groundwater governing equation with one addition advection term

$$\nabla\cdot[K(h)\nabla\lambda] + \left[\varepsilon S_s + C(h)\right]\frac{\partial\lambda}{\partial t'} - \frac{\partial K(h)}{\partial h}\nabla\lambda\nabla(h+z) + \frac{\partial O\delta(x-x_0, t_{final}-t'-t_0)}{\partial h}$$

$$= 0$$

Subject to boundary and final time conditions to adjoint variable field

$$\lambda = 0 \quad \text{at} \quad t = t_{final}$$

$$\lambda = 0 \quad \text{at} \quad \Gamma_1$$

$$K(h)\nabla\lambda = 0 \quad \text{at} \quad \Gamma_2$$

Since

$$\frac{\partial(h+z)}{\partial h} = 0$$

$$\int_\Gamma \lambda\phi\frac{\partial K(h)}{\partial h}\nabla(h+z)d\Gamma$$

$$= \int_\Gamma \lambda\phi[\frac{\partial K(h)}{\partial h}\nabla(h+z) + K(h)\nabla\frac{\partial(h+z)}{\partial h}]d\Gamma$$

$$= \int_\Gamma \lambda\phi\frac{\partial[K(h)\nabla(h+z)]}{\partial h}d\Gamma$$

$$= \int_\Gamma \lambda\phi\frac{\partial q}{\partial h}d\Gamma = 0 \quad \text{at} \quad \Gamma_2$$

With the set of boundary conditions, [6] reduces to

$$\frac{DG}{D\alpha_k}$$

34

$$= \iint_{T\ \Omega} \left\{ \frac{\partial G}{\partial \alpha_k} - \frac{\partial K(h)}{\partial \alpha_k} \nabla\lambda\nabla(h+z) - \frac{\partial[\varepsilon S_s + C(h)]}{\partial \alpha_k}\frac{\partial h}{\partial t}\lambda - \frac{\partial Q}{\partial \alpha_k}\lambda \right\} d\Omega dT$$
$$+ \int_{\Omega} [\varepsilon S_s + C(h)]\lambda\phi\big|_{t=0}\, d\Omega \qquad [7]$$

When calculating the sensitivity using adjoint method for observations at the same location and different times under saturated condition, the adjoint equation only needs to be solved at the terminal time step (the final time step of forward simulation). That is because *K(h)* and *C(h)* do not change with time. For variably saturated case, we should solve the adjoint equation for every observation and every time step respectively.

All terms are readily solved except the last term. If the initial head field is independent of transmissivity, such as the case with hydrostatic initial head, $\phi\big|_{t=0} = 0$.

Otherwise, $\phi\big|_{t=0} \neq 0$ [Lu et. al. 2015]. In order to evaluate this term, assuming that the initial head field, $h_0(\mathbf{x})$, satisfies the steady state flow equation (i.e. head are under steady condition.).

$$\nabla[K(h_0)\nabla(h_0+z)] - Q_0 = 0$$

Following the previous procedure, i.e., taking the derivative of steady state flow equation with respect to the parameter α_k, multiplying both sides of the equation with an arbitrary adjoint variable λ^*, integrating it over the simulation domain Ω, and applying Green's identities, we obtain the adjoint integration term

$$\int_{\Omega} \phi_0 \nabla\cdot[K(h_0)\nabla\lambda^*] - \frac{DK(h_0)}{D\alpha_k}\nabla\lambda^*\nabla(h_0+z) - \lambda^*\frac{\partial Q_0}{\partial \alpha_k}\, d\Omega$$
$$+ \int_{\Gamma} \lambda^* K(h_0)\nabla\phi_0 - \phi_0 K(h_0)\nabla\lambda^* + \lambda^*\frac{DK(h_0)}{D\alpha_k}\nabla(h_0+z)\, d\Gamma$$
$$= \int_{\Omega} \phi_0 \nabla\cdot[K(h_0)\nabla\lambda^*] - \frac{\partial K(h_0)}{\partial \alpha_k}\nabla\lambda^*\nabla(h_0+z) - \phi_0\frac{\partial K(h_0)}{\partial h_0}\nabla\lambda^*\nabla(h_0+z) - \lambda^*\frac{\partial Q_0}{\partial \alpha_k}\, d\Omega$$
$$+ \int_{\Gamma} \lambda^* K(h_0)\nabla\phi_0 - \phi_0 K(h_0)\nabla\lambda^* + \lambda^*\frac{\partial K(h_0)}{\partial \alpha_k}\nabla(h_0+z) + \phi_0\lambda^*\frac{\partial K(h_0)}{\partial h_0}\nabla(h_0+z)\, d\Gamma$$

$$= 0$$

Adding the adjoint integration term into [7]

$$\frac{DG}{D\alpha_k}$$

$$= \iint_{T \, \Omega} \{\frac{\partial G}{\partial \alpha_k} - \frac{\partial K(h)}{\partial \alpha_k} \nabla \lambda \nabla (h+z) - \frac{\partial [\varepsilon S_s + C(h)]}{\partial \alpha_k} \frac{\partial h}{\partial t} \lambda - \frac{\partial Q}{\partial \alpha_k} \lambda\} d\Omega dt$$

$$+ \int_{\Omega} [\varepsilon S_s + C(h)] \lambda \phi \big|_{t=0} \, d\Omega$$

$$+ \int_{\Omega} \phi_0 \nabla \cdot [K(h_0) \nabla \lambda^*] - \frac{\partial K(h_0)}{\partial \alpha_k} \nabla \lambda^* \nabla (h_0 + z) - \phi_0 \frac{\partial K(h_0)}{\partial h_0} \nabla \lambda^* \nabla (h_0 + z) - \lambda^* \frac{\partial Q_0}{\partial \alpha_k} d\Omega$$

$$+ \int_{\Gamma} \lambda^* K(h_0) \nabla \phi_0 - \phi_0 K(h_0) \nabla \lambda^* + \lambda^* \frac{\partial K(h_0)}{\partial \alpha_k} \nabla (h_0 + z) + \phi_0 \lambda^* \frac{\partial K(h_0)}{\partial h_0} \nabla (h_0 + z) d\Gamma$$

$$= \iint_{T \, \Omega} \{\frac{\partial G}{\partial \alpha_k} - \frac{\partial K(h)}{\partial \alpha_k} \nabla \lambda \nabla (h+z) - \frac{\partial [\varepsilon S_s + C(h)]}{\partial \alpha_k} \frac{\partial h}{\partial t} \lambda - \frac{\partial Q}{\partial \alpha_k} \lambda\} d\Omega dt$$

$$+ \int_{\Omega} \phi_0 \{[\varepsilon S_s + C(h_0)] \lambda + \nabla \cdot [K(h_0) \nabla \lambda^*] - \frac{\partial K(h_0)}{\partial h_0} \nabla \lambda^* \nabla (h_0 + z)\} d\Omega$$

$$+ \int_{\Omega} -\frac{\partial K(h_0)}{\partial \alpha_k} \nabla \lambda^* \nabla (h_0 + z) - \lambda^* \frac{\partial Q_0}{\partial \alpha_k} d\Omega$$

$$+ \int_{\Gamma} \lambda^* K(h_0) \nabla \phi_0 - \phi_0 K(h_0) \nabla \lambda^* + \lambda^* \frac{\partial K(h_0)}{\partial \alpha_k} \nabla (h_0 + z) + \phi_0 \lambda^* \frac{\partial K(h_0)}{\partial h_0} \nabla (h_0 + z) d\Gamma$$

[8]

Applying the boundary conditions

$$\phi_0 = \phi(\mathbf{x}, t_0) = \frac{\partial \hat{H}_0}{\partial \alpha_k} \Big|_{\Gamma_1} = \frac{\partial \hat{H}(\mathbf{x}, t_0)}{\partial \alpha_k} \Big|_{\Gamma_1} = 0 \quad \text{on} \ \ \Gamma_1$$

$$-[\frac{\partial K(h_0)}{\partial \alpha_k} \nabla (h_0 + z) + K(h_0) \nabla \phi_0] \cdot n_j = \frac{\partial \hat{q}_0}{\partial \alpha_k} = 0 \quad \text{on} \ \ \Gamma_2$$

Set adjoint variable λ^* to a specific field satisfying the following adjoint equation

$$\{[\varepsilon S_s + C(h_0)] \lambda + \nabla \cdot [K(h_0) \nabla \lambda^*] - \frac{\partial K(h_0)}{\partial h_0} \nabla \lambda^* \nabla (h_0 + z)\}$$

$$= \{\nabla \cdot [K(h_0) \nabla \lambda^*] - \frac{\partial K(h_0)}{\partial h_0} \nabla \lambda^* \nabla (h_0 + z) + [\varepsilon S_s + C(h_0)] \lambda\}$$

$$= \text{diffusion term} + \text{advection term} + \text{source/sink term}$$

$$= 0$$

Subject to boundary conditions to adjoint variable field

$$\lambda^* = 0 \quad \text{at} \ \ \Gamma_1$$

$$K(h_0) \nabla \lambda^* = 0 \quad \text{at} \ \ \Gamma_2$$

Since

$$\frac{\partial(h_0 + z)}{\partial h_0} = 0$$

$$\int_\Gamma \lambda^* \phi_0 \frac{\partial K(h_0)}{\partial h_0} \nabla(h_0 + z) d\Gamma$$

$$= \int_\Gamma \lambda^* \phi_0 [\frac{\partial K(h_0)}{\partial h_0} \nabla(h_0 + z) + K(h_0) \nabla \frac{\partial(h_0 + z)}{\partial h_0}] d\Gamma$$

$$= \int_\Gamma \lambda^* \phi_0 \frac{\partial[K(h_0)\nabla(h_0 + z)]}{\partial h_0} d\Gamma$$

$$= \int_\Gamma \lambda\phi \frac{\partial q}{\partial h} d\Gamma = 0 \quad \text{at} \quad \Gamma_2$$

[8] reduces to

$$\frac{DG}{D\alpha_k}$$

$$= \int_T \int_\Omega \{\frac{\partial G}{\partial \alpha_k} - \frac{\partial K(h)}{\partial \alpha_k} \nabla \lambda \nabla(h + z) - \frac{\partial[\varepsilon S_s + C(h)]}{\partial \alpha_k} \frac{\partial h}{\partial t} \lambda - \frac{\partial Q}{\partial \alpha_k} \lambda\} d\Omega dT$$

$$+ \int_\Omega -\frac{\partial K(h_0)}{\partial \alpha_k} \nabla \lambda^* \nabla(h_0 + z) - \lambda^* \frac{\partial Q_0}{\partial \alpha_k} d\Omega$$

[9]

which is the sensitivity obtained by adjoint method.

The sensitivities of observed head with respect to $\alpha_k = [\ln K_s, \ln S_s, \ln \alpha, \ln n]$

are as following. i represents i[th] observation while k represents k[th] element.
The sensitivity of h to $\ln K_s$ for transient state is

$$\frac{\partial h_i}{\partial \ln K_s^k} = \int_T \int_{\Omega_k} -K(h)\nabla\lambda\nabla(h + z)d\Omega dT - \int_{\Omega_k} K(h_0)\nabla\lambda^*\nabla(h_0 + z)d\Omega$$

The sensitivity of h to $\ln K_s$ for steady state is

$$\frac{\partial h_i}{\partial \ln K_s^k} = \int_{\Omega_k} -K(h)\nabla\lambda\nabla(h + z)d\Omega$$

The sensitivity of h to $\ln \alpha$ is

$$\frac{\partial h_i}{\partial \ln \alpha^k} = \int_T \int_{\Omega_k} [-\alpha \frac{\partial K(h)}{\partial \alpha} \nabla\lambda\nabla(h + z) - \alpha \frac{\partial C(h)}{\partial \alpha} \frac{\partial h}{\partial t} \lambda]d\Omega dT$$

$$- \int_{\Omega_k} \alpha \frac{\partial K(h_0)}{\partial \alpha} \nabla\lambda^*\nabla(h_0 + z)d\Omega$$

This is the equation for VGM model since alpha in C(h) and K(h) are treated as the same parameter. For exponential model, the alpha in the moisture capacity curve is treated as different parameter as that in the K(h) curve.
The sensitivity of h to $\ln n$ is

$$\frac{\partial h_i}{\partial \ln n^k} = \int_T \int_{\Omega_k} [-n \frac{\partial K(h)}{\partial n} \nabla \lambda \nabla (h+z) - n \frac{\partial C(h)}{\partial n} \frac{\partial h}{\partial t} \lambda] d\Omega dT$$

$$-\int_{\Omega_k} n \frac{\partial K(h_0)}{\partial n} \nabla \lambda^* \nabla (h_0 + z) d\Omega$$

The sensitivity of h to $\ln S_s$ is

$$\frac{\partial h_i}{\partial \ln S_s^k} = \int_T \int_{\Omega_k} -S_s \frac{\partial h}{\partial t} \lambda d\Omega dT$$

The sensitivity of h to Q (pumping rate) is

$$\frac{\partial h_i}{\partial Q^k} = \int_T \int_{\Omega_k} -\lambda d\Omega dT$$

$$\frac{\partial h_i}{\partial Q^k} = \int_T \int_{\Omega_k} -\frac{\partial Q}{\partial \alpha_k} \lambda d\Omega dT$$

The sensitivity of flux with respect to parameters could be found at Zha et al. (2014).

5. Analysis of Hydraulic Head and River Stage Data

The following section discusses the spatial and temporal groundwater fluctuation under annual and seasonal scales. Two selected unconfined aquifer wells which locate at about 1.0 (Tan-Cian (1-1)) and 15.0 (Si-Hu (1)) kilometers away from the river are utilized to demonstrate the spatial differences of groundwater level variation. Through the spatial, temporal, and groundwater level time frequency analysis, one could roughly figure out the possible correlation between different variables and thus determine the potential subsurface hydraulic parameter distributions.

5.1. Integrated Groundwater Level

To evaluate the general temporal pattern of groundwater level variation during 1998 to 2013, daily groundwater level of unconfined aquifer are integrated together using ordinary kriging. The integrated groundwater level not only represents weighted average groundwater level variation at the alluvial fan, but also could be interpreted as the groundwater storage change if multiplying with the storage related parameter such as porosity of the porous media.

5.2. Scaled Precipitation

Precipitation is a relative discrete time series in comparison with river stage or groundwater level. Discrete signal is difficult to separate into frequency domain when utilizing short term Furrier transform, wavelet analysis, or etc. doing time frequency analysis. This is because the base or mother waves been used in these techniques are periodic waves such as sine or Mexican hat. Thus, transformation of precipitation signal to more continuous periodic form is necessary and could provide advantages for the time frequency analysis.

To obtain the periodic rainfall signal, the first process is integrating the amount of rainfall with time, which yields cumulative rainfall. Then, remove the linear trend by assuming, in average, the precipitation is uniformly distributed along the time domain. That is, each day has the same rainfall amount. This detrended cumulative precipitation provides information about rainfall perturbation above or below the mean (figure 7). Essentially, the peak of detrended cumulative precipitation indicates that it is wetter than the average while the valley indicates it is dryer than the average.
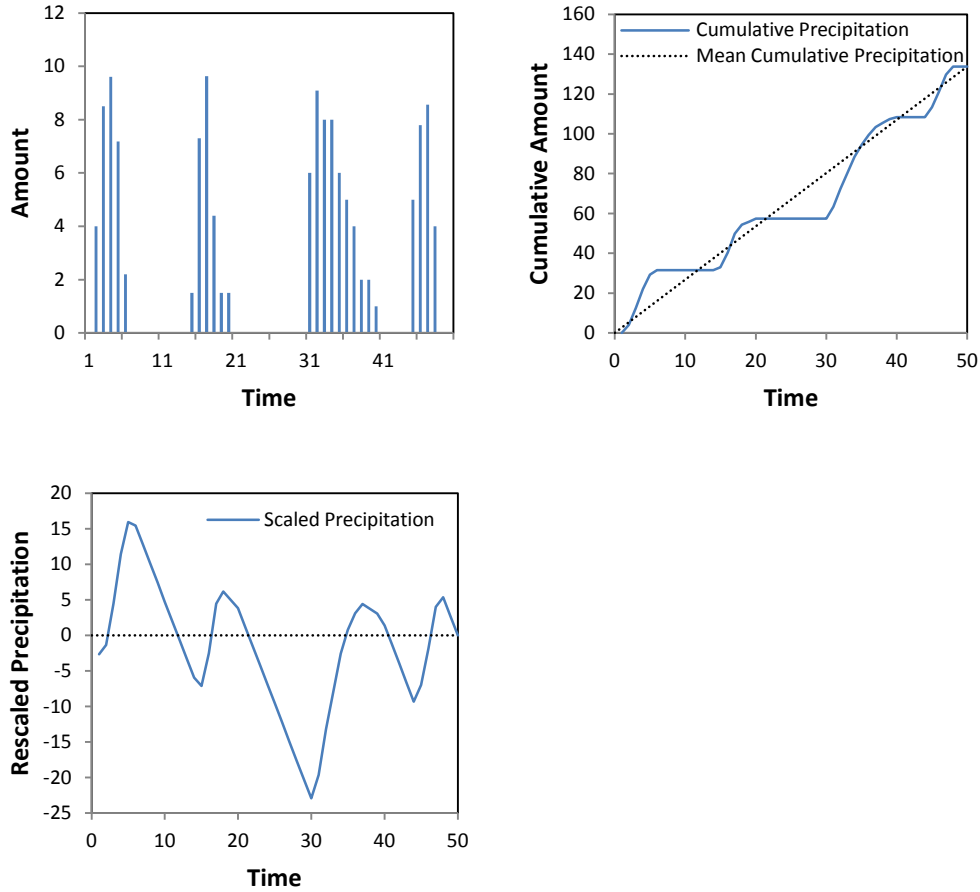
Figure 7. Schematic diagram of a) discrete, b) cumulative, and c) scaled precipitation.

5.3. Spatial and Temporal Groundwater Fluctuation

Before doing quantitative periodic analysis using wavelet, it is better to make sure there're significant periodic cycles during the study time period.

It is observed in the groundwater level contour maps that in the most region of the alluvial fan, the groundwater variation has a significant annual cycle. Groundwater begins to drop from spring and reaches its lowest point at summer then starts to recover. When winter comes, the groundwater level generally is recharged to its original level in the beginning of the year. The drop and recovery of the groundwater level in this area follows the trend of agriculture water demand and the rainfall season (figure 8).

Take groundwater level during 2010 as example. The annual maximum groundwater level drawdown occurs at the southern alluvial fan at May (figure 8). There are two main drawdown regions, the first one locates around San-He station while the other is at Da-Gou and Qiong-Pu stations. The annual maximum drawdown compared with January 1st, 2010 at these two main drawdown regions is about 7 m. The annual maximum groundwater level recovery compared with January

1st, 2010 during the study period (2010) occurs at the apex of the alluvial fan around late October. At Xin-Guang and Xin-Min stations, the maximum recovery is about 5.5 m.

Based on the spatial and temporal groundwater level variation, it could be deducted that the southwest region is a relative pumping heavily demand area while the apex of the fan is probably main recharging region of the aquifer.
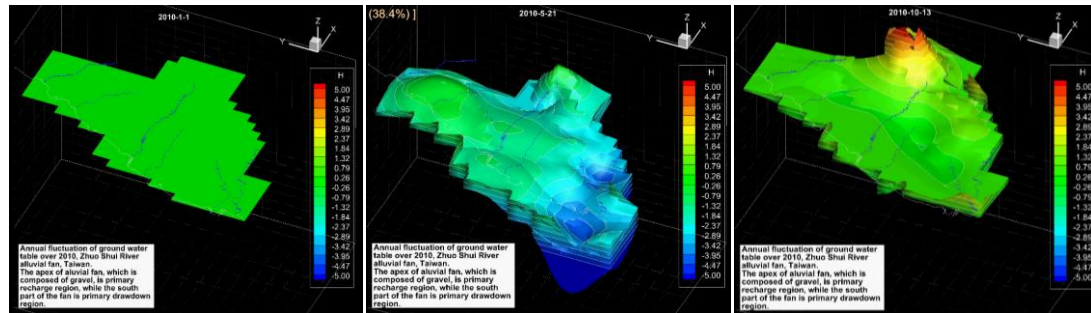

Figure 8. Annual groundwater level variation during 2010. Groundwater levels are set to be zero at January 1st.

5.4. Periodic Analysis

Figure 9 illustrates the daily time series and its associated wavelet spectrograms of integrated groundwater level, scaled precipitation at Chiayi weather station, and river flow rate at Zhangyun Bridge during 1998 to 2013. The power of the real part of wavelet coefficient is equivalent to the power spectrum, or in other word, the relative energy distribution. Spectrogram quantifies the relative energy distribution along the frequency and temporal domain of study area. By analysing the positive-negative value pairs, one could easily recognize the periodic trend of interested variable based on the past record.

It is observed that the integrated groundwater level, scaled precipitation, and flow rate of river during the study period has significant periodic variation on decadal and annual periods. The seasonality variations within 50 to 150 days of period could be observed as well. The strength of decadal and annual periods are much more significant than the seasonal cycle.
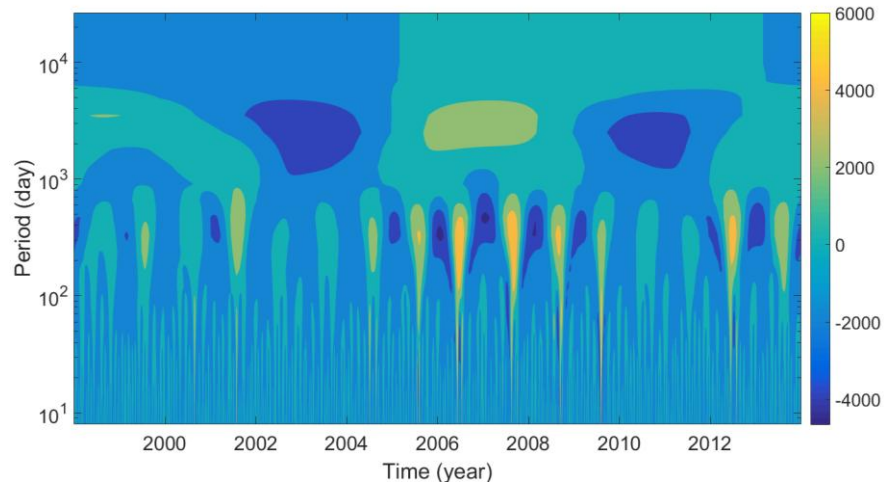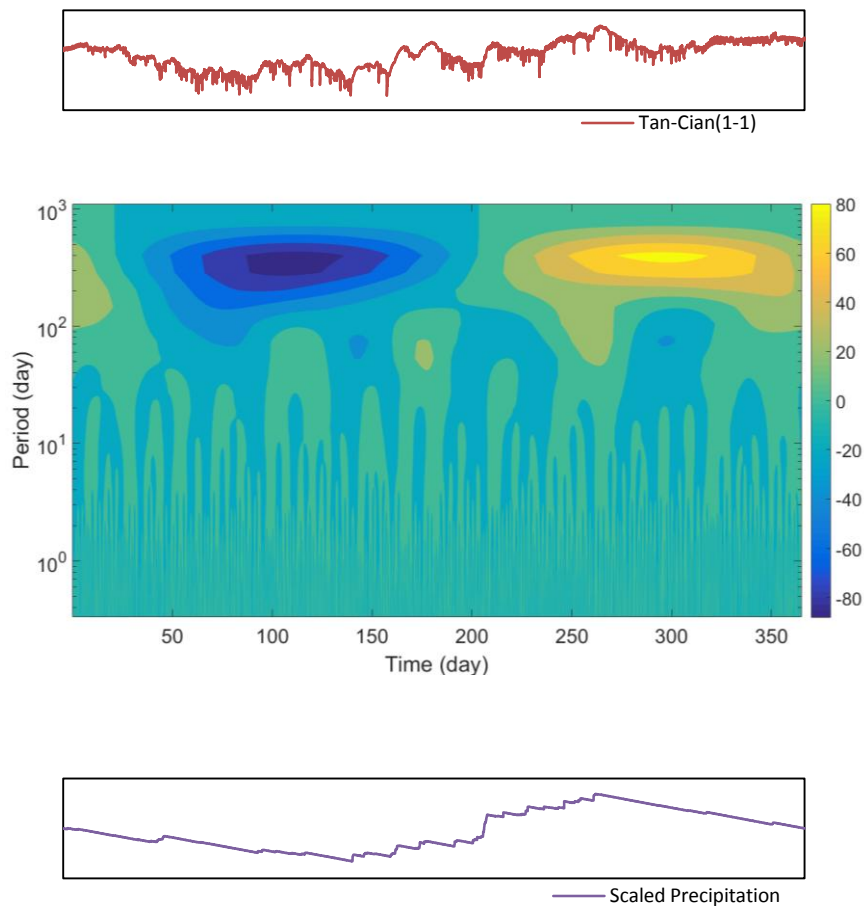

Annual Storage Change
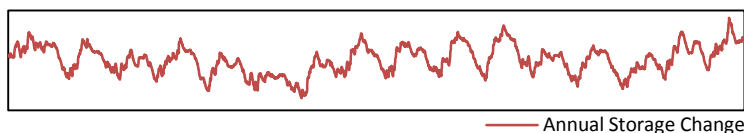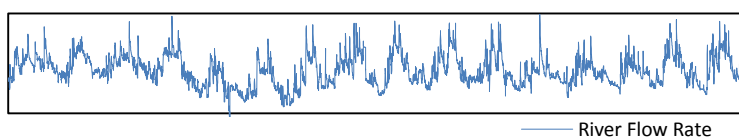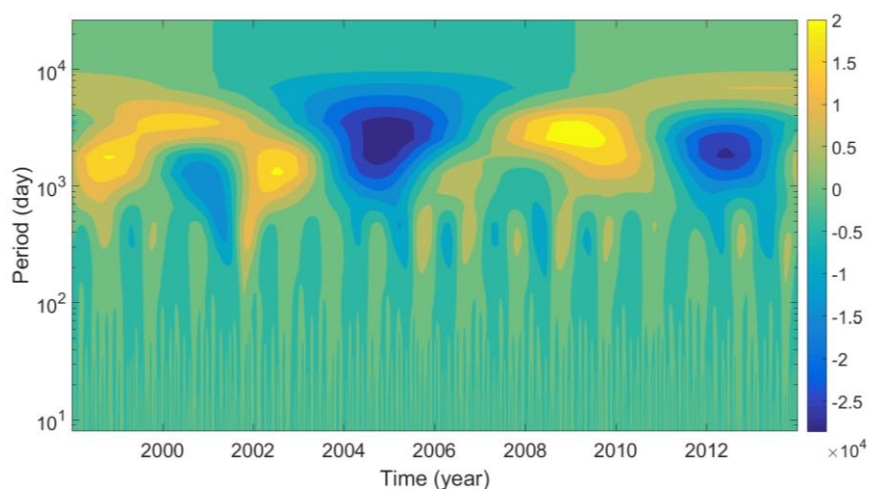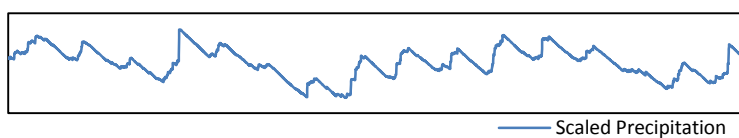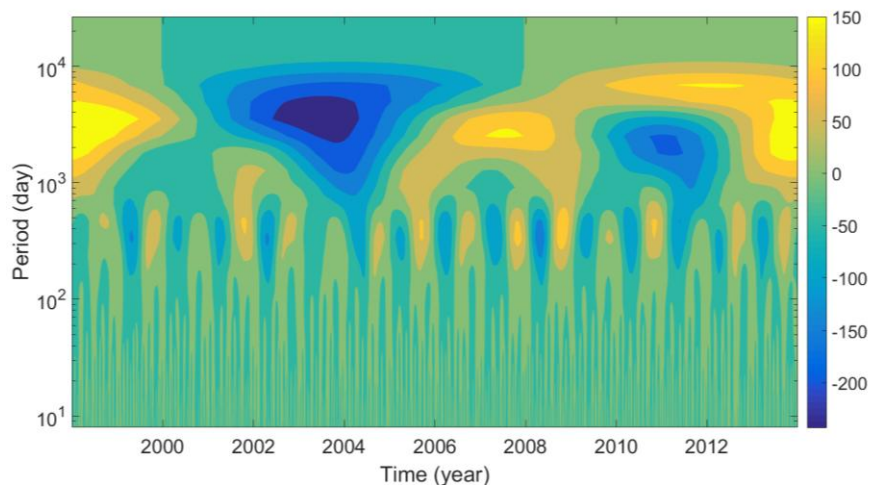
Figure 9. Time series and associated wavelet spectrograms of the a) integrated groundwater level change, b) scaled precipitation at Chiayi, c) river flow rate in $\log_{10}$ scale at Zhangyun Bridge during 1998 to 2013. The contour color represents the real part of wavelet coefficient.

Figure 10. Time series and associated wavelet spectrograms of the a) groundwater level at Tan-Cian (1-1), b) scaled precipitation at Xiashuipu, c) river stage at Ziqiang Bridge during 2010. The contour color represents the real part of wavelet coefficient.

Hourly water level and meteorology data during 2010 are selected as the example to explore the higher frequency signals wh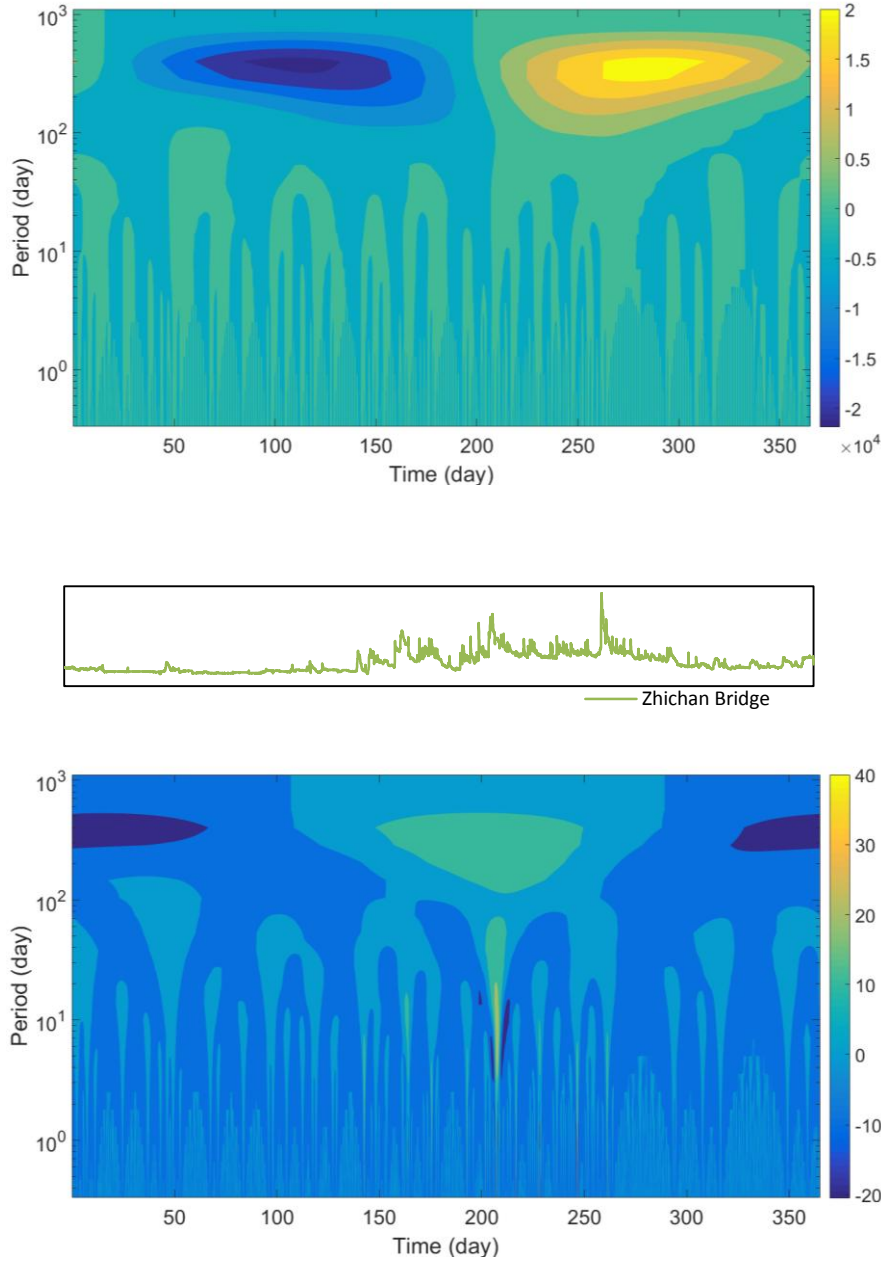ose periods are smaller than 50 days. Figure 10 illustrates the hourly time series and its associated wavelet spectrograms of groundwater level at Tan-Cian (1-1), Si-Hu (1), scaled precipitation at Xiashuipu, and stream stage at Ziqiang Bridge. The actual location of these selected stations could be found in figure 1.

In addition to the annual cycle, the groundwater level at Tan-Cian (1-1) and

Si-Hu (1) has three seasonal periodic cycles with period around 60 to 80 days from April to October. Periodic trend with period smaller than 20 days could be observed all over the year.

Unlike the groundwater level, the scaled precipitation at Xiashuipu does not have significant periodic seasonal variations. Instead, variations with periods less than 40 days take places.

The period cycles of stream stage variation during rainfall season (i.e. April to October) at Ziqiang Bridge are similar with that of the groundwater level at Tan-Cian (1-1) and Si-Hu (1). Periodic trend with period smaller than 20 days could be observed as well.

5.5. Select Time Period with Sufficient Variation

The purpose of the study is to characterize subsurface characteristics by utilizing the information provided by stream induced groundwater level variations. Thus, the selection of time intervals with appropriated criteria is necessary. The first criterion of the selection of time interval is the rising and falling of groundwater level should correlate with stream stage or flow rate variation even though it is at distant location. The second criterion is that since many sources such as pumping, precipitation or river could have contribution to the variation of groundwater level, selection of an appropriate time interval which river is a relative strong source is an important step before the analysis of stream groundwater interaction.

Figure 11 illustrates the separated time series of groundwater level, precipitation, and stream stage or flow rate at periods of daily, weekly, seasonally, and annually at the study site. They are acquired by inverse wavelet transform by keeping the energy at desired periods and setting the else to be zero.

By glance of look, it is likely that at daily and weekly scale (figure 11a and 11b), the groundwater perturbation is uncorrelated or small correlated with the stream stage variation no matter how far away the groundwater monitoring wells are from the stream. The groundwater level is uncorrelated or small correlated with precipitation either.

On the other hand, the seasonal groundwater variation appears to be related to river stage fluctuation (figure 11c). It appears that, in the most part of the study region, begin from late spring till the middle of fall, the variation in groundwater level has a positive correlation with the variation of the river stage with a phase lag about several hours to several days, depending on the location of the well. Take the water levels at two monitoring wells with the different distance to the river as examples. The correlation coefficient between variations of groundwater level and stream stage are 0.64 and 0.53 at monitoring wells 1.0 and 15 km away from the river, respectively,

while the lags of time are 3.2 and 3.1 days. Meanwhile, groundwater level variation is correlated with precipitation as well. The correlation coefficient between variations of groundwater level and stream stage are 0.60 and 0.49 at monitoring wells 1.0 and 15 km away from the river, respectively, while the lags of time are 0.7 and -0.3 days. The groundwater level change in responses to the fluctuation of river stage or rainfall isn't significant in winter. Such behavior might be attributed by the major rainfall season of the study area during the summer, where there are strong connections between the stream and groundwater. Therefore, river induced pressure wave can easily propagate through the aquifer.

Groundwater level has relatively strong correlation with both rainfall and stream flow rate under annual scale (figure 11d) as well. However, the lags of time between groundwater level and rainfall as well as stream flow rate are 160 and -357 hours respectively.

Based on the correlation information provided by time frequency analysis, seasonal and annual scale variations satisfy the criteria that groundwater level variation is correlated with stream stage or flow rate. However, since lags of time at some wells between groundwater level and precipitation at seasonal and annual scales are negative, which represents groundwater level responses earlier than the peak of rainfall event occurred, the correlation between variations of groundwater level and rainfall may be due to other sources such as pumping rate variations. Because the purpose of this study is trying to utilize groundwater level change in response to stream stage variation, seasonal variations during rainfall season which satisfies the two criteria are selected instead of annual, weekly, and daily periods. The selected seasonal variations (Julian day 130-200 and 200-300) will be utilized to characterize subsurface heterogeneity employed by two different approaches.
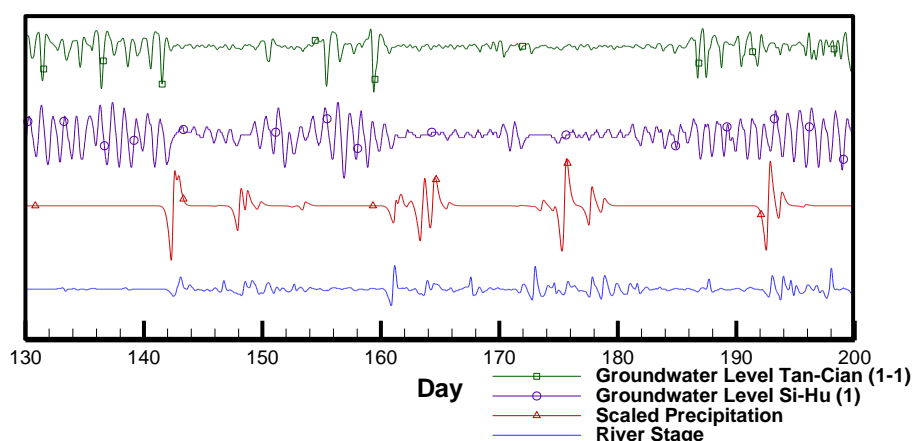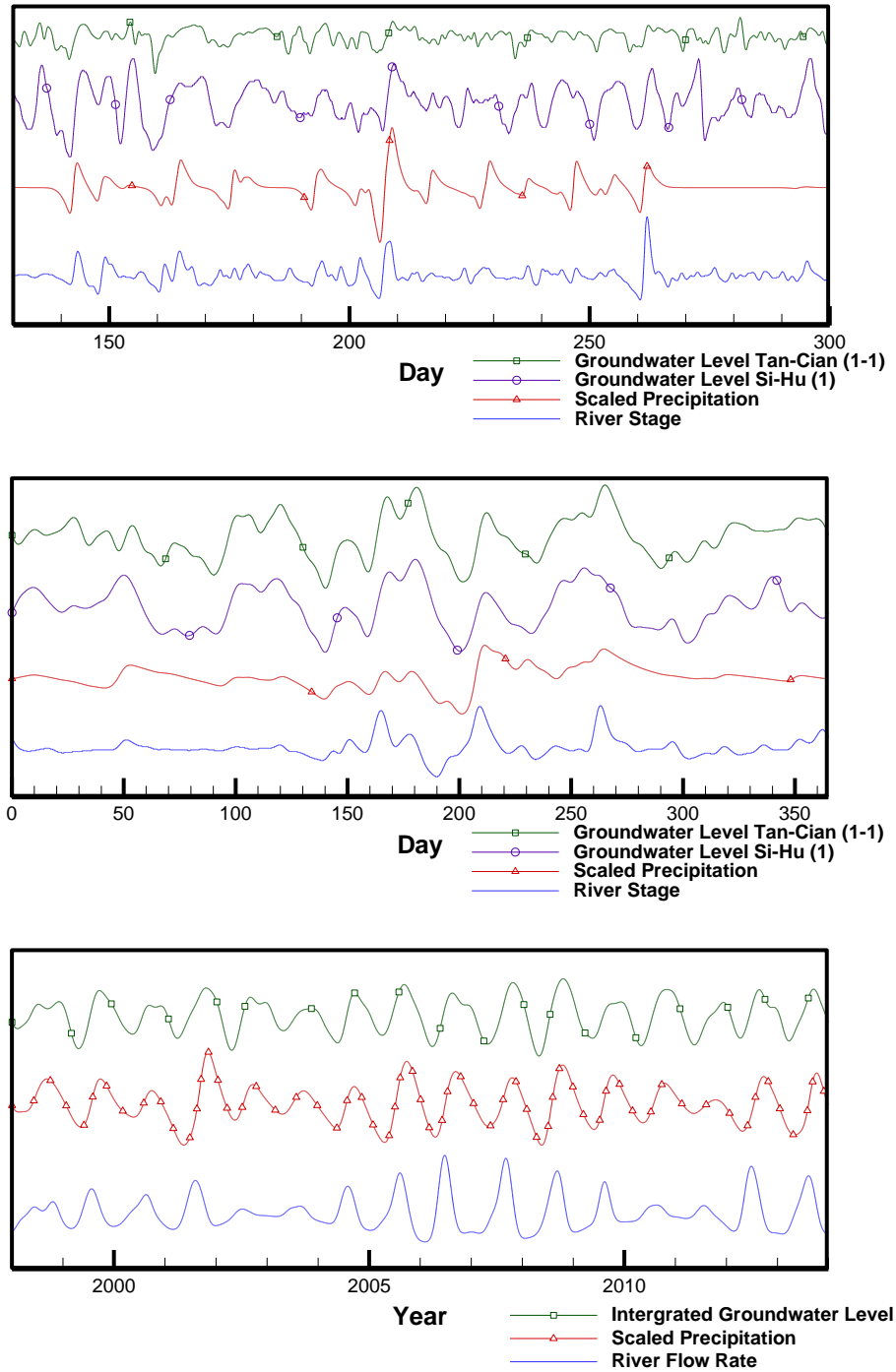
Figure 11. Reconstruct groundwater level at Tan-Cian (1-1), Si-Hu (1), scaled precipitation at Xiashuipu, and river stage at Ziqiang Bridge during 2010 with period of a) 0 - 1.3 days, b) 1.8 - 7.0 days, c) 9.75 - 74.3 days. d) Reconstruct groundwater level, scaled precipitation at Chiayi, and river flow rate at Zhangyun Bridge during 1998 to 2013 with period of 167 - 461 days.
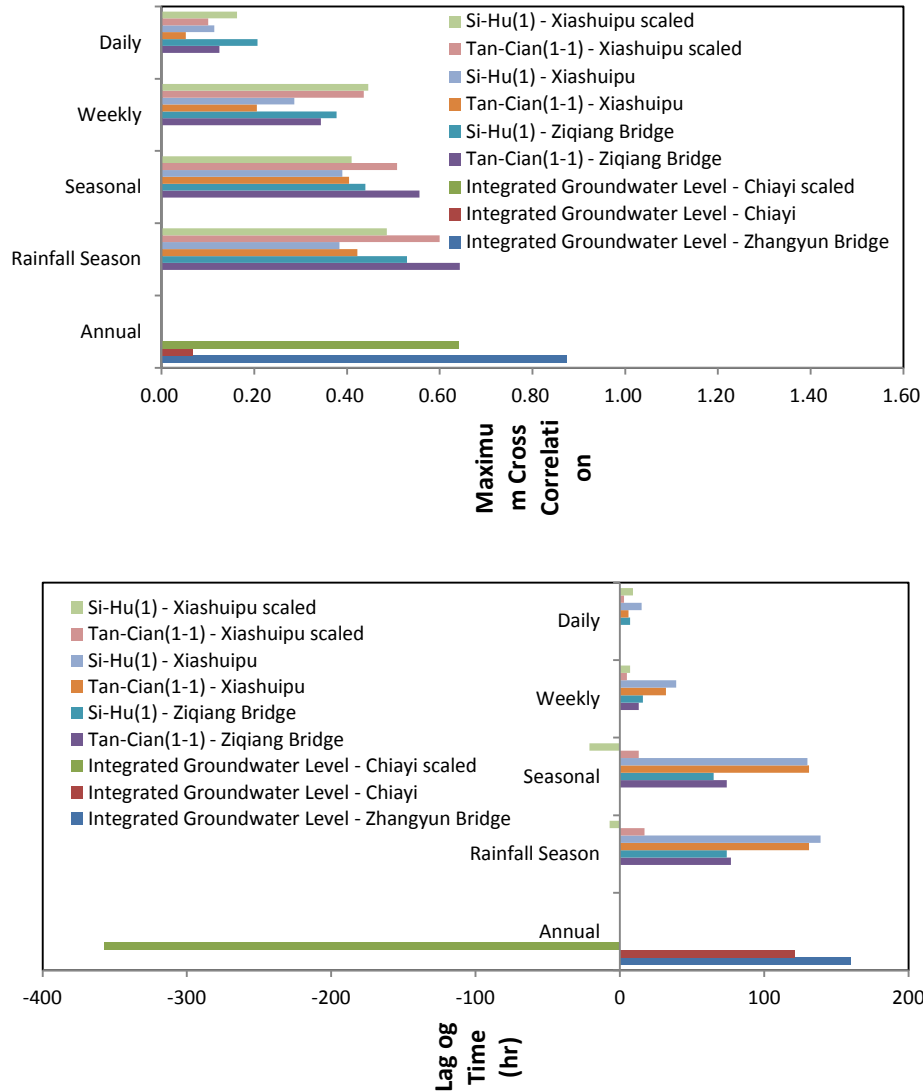
Figure 12. a) Maximum cross correlation and b) associated lag of time between groundwater level (Tan-Cian (1-1) and Si-Hu (1)), precipitation (Xiashuipu and Chiayi), scaled precipitation, and stream stage (Ziqiang Bridge) or flow rate (Zhangyun Bridge) under annual, seasonal, weekly, and daily periods and during rainfall season. Positive time lag represents groundwater level rises later than stream or precipitation while negative represents earlier.

5.6. Generate Spatial Continuous Stream Stage Hydrograph

For the purpose of simulating stream induced groundwater level variation, flows in Zhuoshui River and Wu River are borrowing from the field record from the five stream gauge stations (four at Zhuoshui River and one at Wu River). For Zhuoshui River, because the flood wave propagating from the apex to tail of fan only takes about 8 hours (figure 13) and the distances between gauges ares really short (only about 10 km), the river stages between the two stream gauges are obtained simply by

linear interpolation. For Wu River, because it is only a northern boundary least for about 10 km, the stream stage along the Wu River is simply assumed to be constant head spatially.
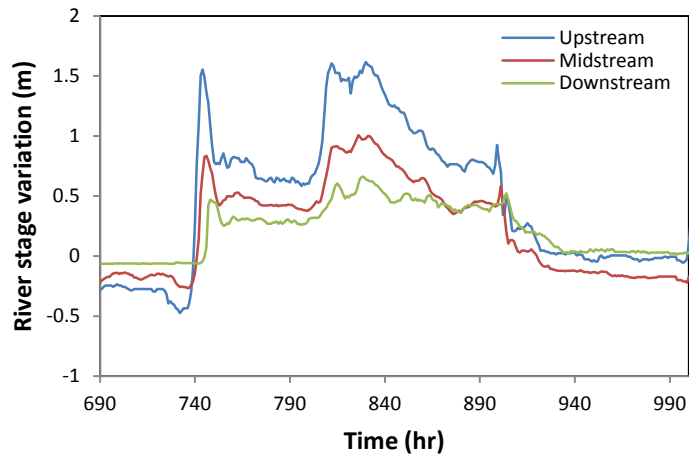

Figure 13. Propagation of the flood wave in the river.

6. Synthetic Experiment

Synthetic experiment is carried out to study the performance of cross correlation and river stage tomography on estimating basin scale spatial Ks distribution. In this section, we will qualitatively and quantitatively describe the Ks distribution along the alluvial fan. The estimated field will be compared with the reference. Then, the improvement of the inclusion of prior geological knowledge to the estimation will be discussed.

6.1. Aquifer Response to Flood

Figure 14 shows the hydrographs recorded at two selected wells which are 1 km (Tan-Cian) and 15 km (Si-Hu) away from the stream, respectively. As expected, observation well closer to the river in the lateral direction responds faster than that located further away from the river as indicated by the arrival time of the peak. Furthermore, irregular shapes of these well hydrographs reflect weighted mixing effects of propagation of the river disturbance as well as aquifer heterogeneity.
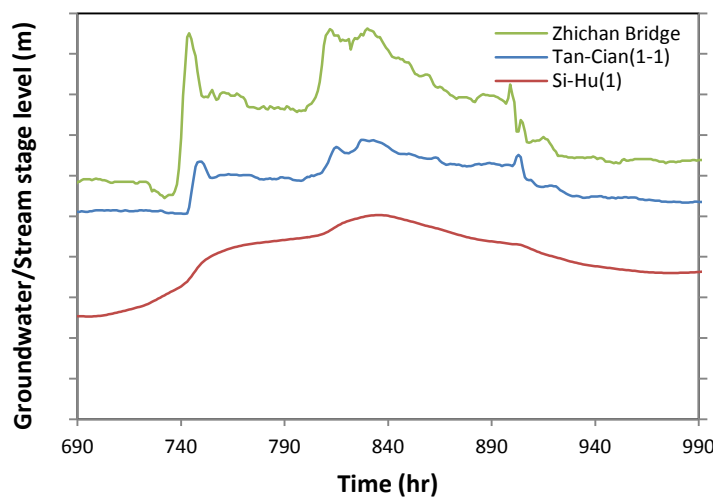
Figure 14. Observed well hydrographs in response to the stream stage variation at two selected locations in the aquifer.

6.2. Estimate of Ks Spatial Distribution

Figure 15 displays the estimated Ks distribution obtained from cross correlation analysis and river stage tomography (scenario 1) using hydrographs from the observed wells during the selected seasonal variation. Scatter plot of reference versus estimated value of Ks is shown in figure 14 as well.

At first glance of the estimated Ks fields, each of them apparently captures the general pattern of the reference field. In figure 15a, clusters with similar cross correlation occupy the apex of the fan as well as area near the northern boundary.

Meanwhile, cross correlation values along the southern alluvial fan are similar. Furthermore, in figure 15b, the relative high K zones (red) occupy the apex of the fan and region around the northern boundary while the relative low K zones (blue) extend throughout the southern part of alluvial fan. Noticeably, these patterns are not restricted to the areas closer to the wells or the time varying river boundary where heads were observed and used in the estimation. They also cover areas far away from the wells or near the boundaries of the aquifer. This phenomenon indicates that the head at a specific point within an aquifer during the flood event is affected by subsurface hydraulic properties even far away from the observation and near the boundary where stream induced groundwater variations displayed.

A second look at the contour maps reveals that each estimated field is different from the others even though all estimated fields bear some similarities. Since the reference field is known, the performance statistics (slope and R^2) for the comparison between the reference field and each estimated field are show in scatter plots. The slope of river stage tomography regression line is 0.36 while that of cokriging is 0.14. The slope closer to 1.0 indicates the estimate is closer to the reference. It reveals river stage tomography approach could characterize the hydraulic property more detailed, thus has better spatial resolution. The correlation coefficients, R^2, are 0.77 and 0.57 for river stage tomography and cokriging respectively. Values of R^2 also suggest river stage tomography could yield the estimate more correlated with the reference field. Notice that the head data of the synthetic aquifer is free of measurement and physical model errors, and there is no uncertainty in the boundary condition and unknown pumping in the inverse modeling effort.

Distributions of the residual variances (estimate uncertainty) of the estimated Ks are shown in Figures 16. These figures show that the residual variances of hydraulic conductivity field estimated from cokriging generally increase as the distance to the river increases. On the other hand, the residual variances estimated from river stage tomography increase as the distance to the monitoring well increases. That is, the shorter the distance between the well or flood disturbance, the smaller the uncertainty of the estimate, and the longer the distance, the larger the uncertainty of the estimate. Moreover, the uncertainty of the river stage tomography estimation is smaller than that of cokriging because river stage tomography conditions estimated Ks field with the measurement heads.
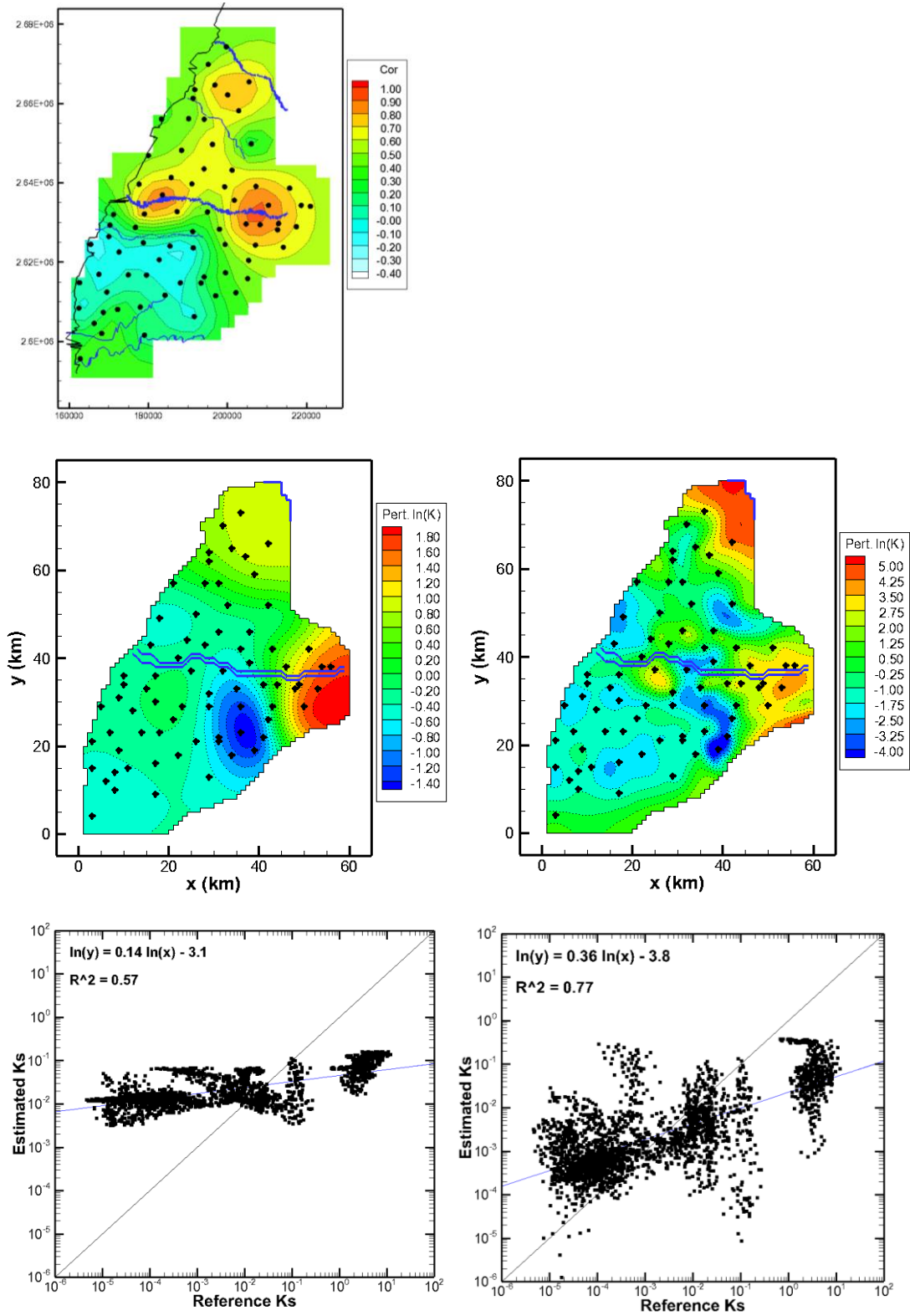
Figure 15. a) Cross correlation contour map. b) Hydraulic conductivity estimation fields and c) associated scatter plot of reference versus estimated value obtained from cokriging and from d,e) river stage tomography starting from uniform mean. Legend

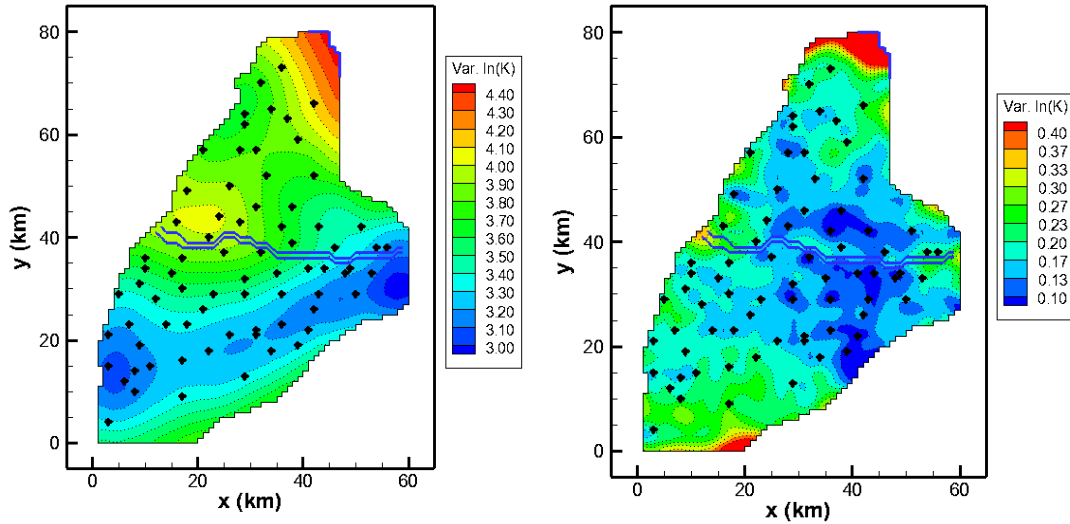*Pert.* $\ln(K) = \ln K_s - \ln \overline{K}_s$.

Figure 16. Residual variance (estimate uncertainty) of the estimated hydraulic conductivity obtained from a) cokriging and b) river stage tomography starting from uniform mean.

6.3. Effect of Prior Geological Information to the Parameter Estimation

Figure 17 displays the estimate fields and associated performance scatter plots using river stage tomography with known (scenario 2) and unknown (scenario 3) zone boundaries. When the prior geological knowledge are included, the bias and errors of the estimates both drop. The reduction is reflected in slope and R^2 of linear regression line between estimate and reference Ks. Compared with scenario without any geological knowledge (scenario 1), the slope increases from 0.36 to 0.94 and 0.61 for known (scenario 2) and guess (scenario 3) boundary respectively. Correlation coefficients R2 improve from 0.77 to 0.98 and 0.83 as well. The improvement of the estimation reveals that the use of zonation as prior information allows groundwater flow equation to closely reproduce the head field, such that the final estimations of each zone could present mean value closer to true mean in the reference field.

It is also observed that although the overall estimate is improved if including the potential spatial Ks distribution as the prior information, it is likely that there are more over and underestimated Ks deviating away from the 45 degree line. This may be because if the initial gauss of mean is too far away from the true mean, due to the lack of knowledge to the site, it is difficult for simSLE algorism to adjust the Ks to the appropriate order of magnitude since there're many possibilities or realizations that estimated heads could satisfy observed heads.

The residual variances estimated from river stage tomography increase as the distance from the observation wells increases. The uncertainty near the boundary is relatively larger (figure 18).
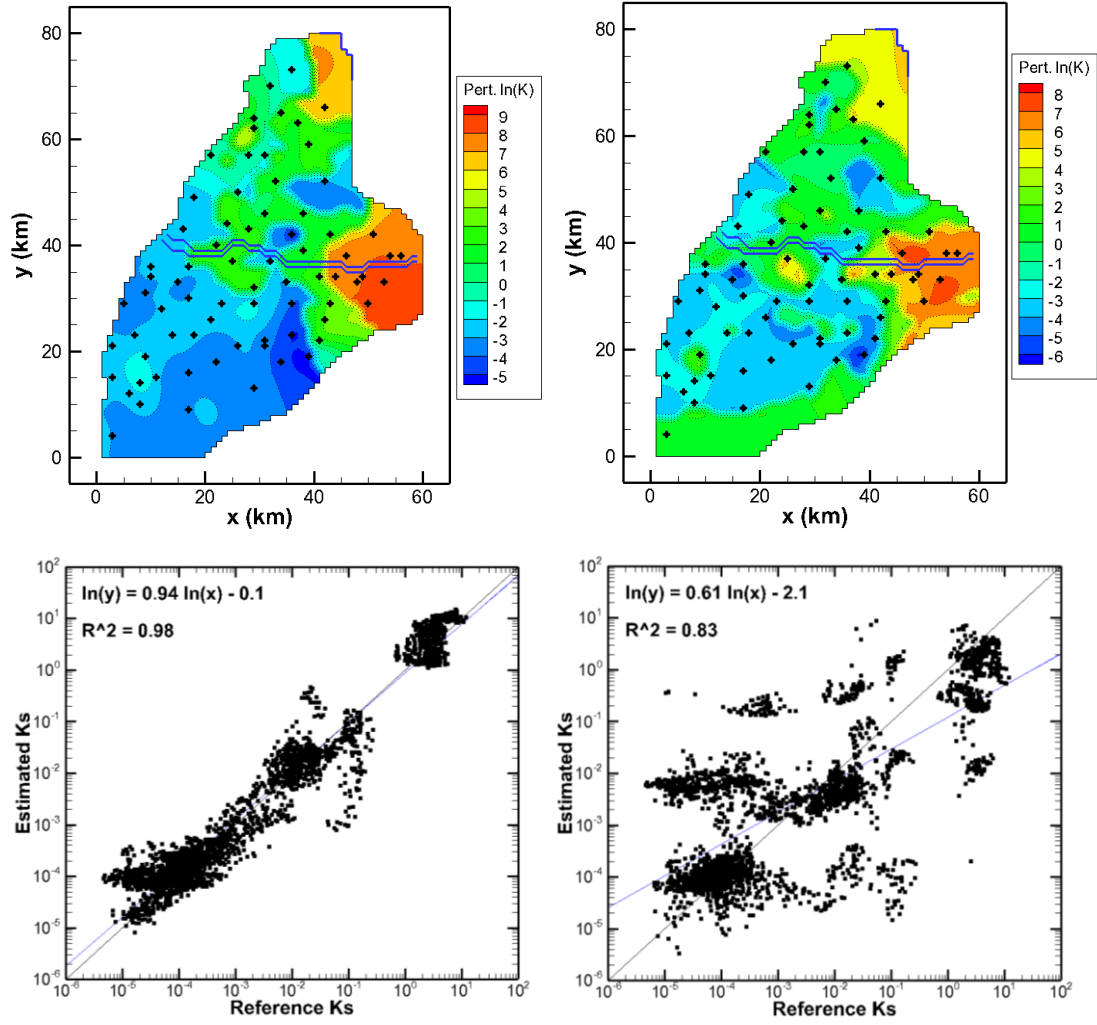
Figure 17. Hydraulic conductivity estimation fields and associated scatter plot of reference versus estimated value obtained from river stage tomography starting from a) true distributed mean and b) guess distributed mean.
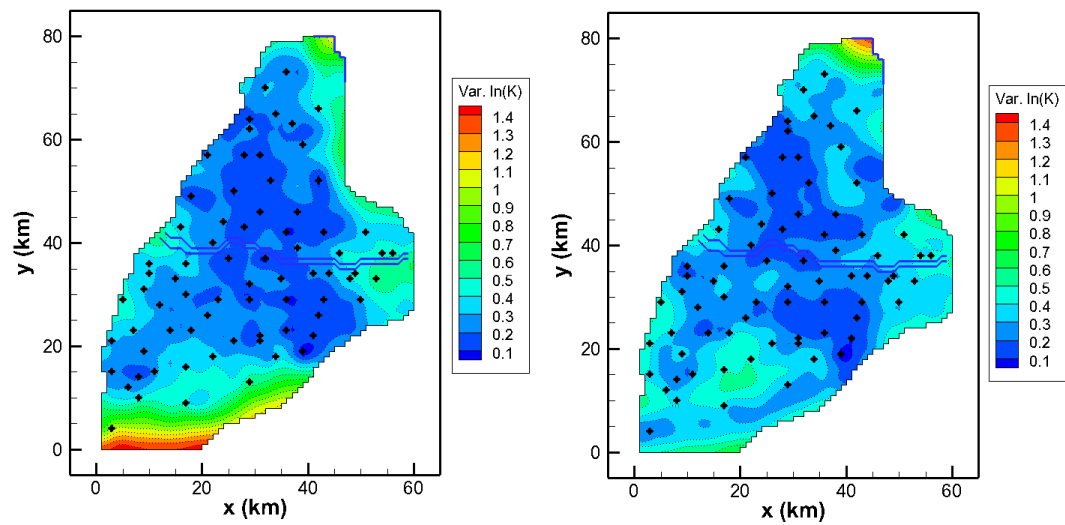

Figure 18. Residual variance (estimate uncertainty) of the estimated hydraulic

conductivity obtained from river stage tomography a) starting from true distributed mean and b) starting from guess distributed mean.

7. Implement to Zhuoshui River Alluvial Fan

It has been demonstrated and concluded by synthetic experiment that cross correlation, cokriging, and river stage tomography could identify the subsurface heterogeneity out in different resolution under basin scale. The next step is to implement these techniques to field problem.

7.1. Spatial Distribution of the Cross-Correlation

Figure 19a illustrates the cross correlation contour maps of seasonal variations during 2010.

The cross correlation result indicates that there are two areas where groundwater level is highly correlated with stream stage variation at Zhuoshui River alluvial fan. The first one, whose maximum cross correlation is about 0.7, locates at the north side of the fan and has highest cross correlation around Hua-Tan station. The second one, whose maximum cross correlation is also about 0.7, locates at the south of the fan around Fang-Cao station.

The spatial distribution of maximum cross correlation suggests that groundwater fluctuation in the area locates at the northern and the tail of the fan near the river tends to be highly positive correlated with the river stage variation. In the apex of the alluvial fan, groundwater fluctuations are always negative or uncorrelated with the river variation. Southeast part of the fan is an uncorrelated or small correlated region.

Figure 19b illustrates the lag of time associated with the cross correlation contour map. Lag of time is an index describing the time interval before the recharge reaches groundwater table or stream induced pressure wave arrives. It is observed that at the apex of the fan, it will take about 15 days for the vertical infiltration percolating through the subsurface and recharging the aquifer.

In summary, at apex of the fan, variation of groundwater level is small or none correlated with variation of stream stage along with long time lag. At the rest of the region, the correlation between stream stage and groundwater level are relative higher along with relative shorter lag of time.
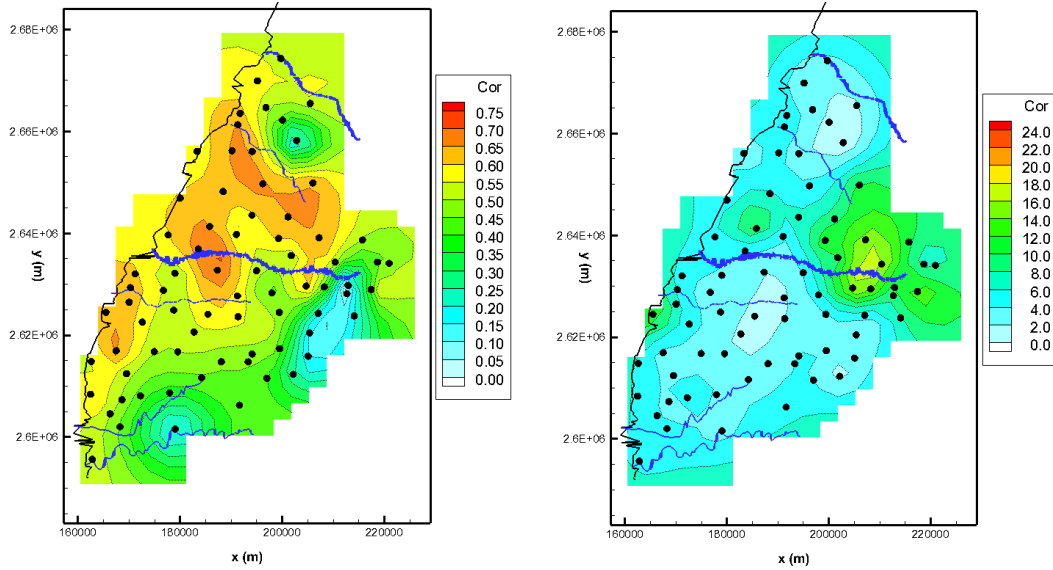
Figure 19. a) Maximum cross correlation and b) associated time lag fields 40 m below the sea level obtained from the seasonal river stage variation events (Julian day 130-200).

7.2. Spatial Distribution of estimated Ks Field by Cokriging

Figure 20 illustrates the estimated Ks fields and associated estimate uncertainty by cokriging. It is estimated that the spatial Ks follows high to low pattern from the apex to tail of the fan as well as from the north to the south.

7.3. Similarities between Maps Obtained from Two Approaches

The estimated fields obtained from these two approaches remain some similarities. For example, it is observed that the apex of the fan has its unique subsurface characteristic because the lag of time is relative longer in comparison with middle and tail. It is also observed that there are patterns both from the apex to tail and from north to south. These similarities and their associated physical meanings or subsurface representations will be discussed.

The resolutions of estimate field using field data are different between two approaches and are identical with those using synthetic data. In synthetic experiment, it is concluded that cokriging approach could yield estimated Ks field more detailed compared with that from cross correlation if the measurements are noise free. However, in field experiment, the estimate resolution is likely opposite. Cross correlation characterizes the subsurface heterogeneity more detailed than cokrig does.
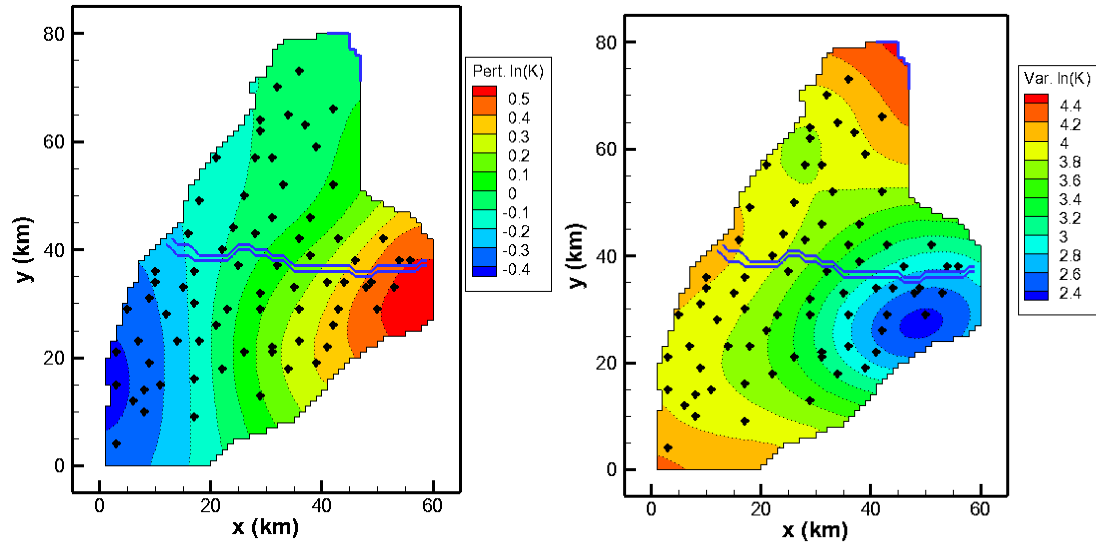
Figure 20. a) Hydraulic conductivity estimation fields obtained from cokriging and b) associated residual variance (estimate uncertainty) during the selected seasonal variation.

8. Discussion

Evaluation of the estimate fields obtained from different approaches by synthetic experiment suggests that one could identify the general spatial pattern of Ks distribution in a groundwater basin by both cross correlation and river stage tomography techniques. However, river stage tomography could characterize the Ks field more detailed such as area bounded by relative high K zone at northeast side of the alluvial fan. In comparison with cokriging, river stage tomography could dig into and resolve more information that is carried by observed data.

Furthermore, it is observed that with the knowledge of prior geological information, the estimated Ks field could be improved. The improvement of estimates is not limit to the domain near boundary where none or less observation is made. The prior knowledge enhances the estimates within the wells as well.

Although the overall estimate is improved if the possible spatial Ks distribution is included, it is observed in figure 17d that some estimations deviating away from the 45 degree line. These over or underestimated Ks may be attributed to the introduction of poor quality prior information. That is, if the initial guess of ensemble mean is incorrect or too far away from the true one, although the spatial pattern of estimated field could still be caught, the estimated value won't be correct. In other word, if we overestimate the initial mean of a relative high K zone, in order to balance out this effect, the final estimated Ks of the surrounding relative low K zone will be underestimated. The synthetic experiment reveals that the poor prior knowledge is worse than without any. Thus, it is suggested if we are not really sure where the border regions of nearby zones are, it is better to set the initial guess of Ks around these border areas to ensemble mean.

Field data carry bunch of information about the study site. The similarity of the estimated fields from approach 1 and 2 suggests that the apex of the fan has its unique subsurface characteristic. This characteristic is significantly different than those at middle and tail of the fan. The difference and uniqueness could be observed in figure 19 that in the apex of the alluvial fan, groundwater fluctuations are always negative or uncorrelated with the river stage variation along with a pretty long lag of time about half of the month. While at the other region of the fan, the time lags are essentially shorter than 5 days with positive correlation. Such a long lag of time at the apex of the fan could be attributed to the sediment size and depth of the groundwater table. Based on the well logs survey, the apex mainly consists of coarse gravel while the groundwater table is at 30 m depth below ground surface. The tortuous preferential flow pathways through the coarse grain vadose zone not only filter out the high frequency signal but also delay the movement of wetting front. Thus, both small or uncorrelated correlation and long time lag are observed in the apex area. The relative

high Ks zone estimated by cokrig (approach 2) also agrees with this idea. It should be noted that the Ks value at the apex might be underestimated. Because in this study we utilize 2D model to simulate groundwater flow, which already automatically assumes the stream connects to the groundwater table perfectly, groundwater level will response to stream stage change immediately. The ignorance of percolation time delay due to the unsaturated region leads to the fact of underestimated Ks since simulated heads need to satisfy the lags of time in observed groundwater heads in response to stream stage variation.

The similarity between two approaches also reveals a general Ks pattern from the apex till the tail. Based on the estimated field by cokrig, it is likely that region at the apex is a relative high Ks zone while middle is intermediate Ks and tail is relative low Ks area respectively. This spatial Ks pattern agrees with the conclusion of well log survey that apex mainly consists of gravel and following with middle and tail of the fan are consist of sand and silt/clay.

It is also observed that the subsurface characteristic at northern alluvial fan differs from the southern part as well. The estimated Ks are relative larger at north than at south. This finding agrees with Tsai et al. (2016)'s conclusion. Tsai et. al. integrate the well log with electric resist survey utilizing apparent model technique. They find that the northern part of alluvial fan is mainly in sand along with some silt/clay layer along the coast while the southern fan is mainly in silt/clay.

It is interesting that why the estimated Ks at northern alluvial fan are larger than southern. Since it is suggested that grain size at northern alluvial fan is larger than the southern, if we attribute the grain size difference to the fact of sediment source difference, it could deduct that the southern alluvial fan is mainly deposited by the Beigang River, while the northern fan is mainly deposited by Zhuoshui River. In other word, during the past, Zhuoshui River probably only mainly flew through the northern. The deduction is reasonable because since Zhuoshui River is originated from Central Mountain Range and has steeper river bed gradient, sediment transported by the river could carry not only sand but also gravel. On the other hand, Beigang River originates from Douliu Hills and has smoother gradient, thus only sediment size smaller than sand could be transported. (Water Resources Agency, 2014)

9. Conclusion

For the purpose of managing groundwater resources and controlling the regional land subsidence over the Zhuoshui River alluvial fan to prevent seawater intrusion, it is necessary to regulate the number of pumping wells as well as pumping rates. To evaluate the drawdown cones introduced by pumping activity, subsurface hydraulic parameter distribution such as hydraulic conductivity, K, should be determined.

In this study, we utilize three approaches, cross correlation, cokriging, and river stage tomography, to study and estimate the spatial Ks distribution along the Zhuoshui River alluvial fan, Taiwan.

The synthetic experiment reveals that all of the approaches could estimate the general spatial K distribution. While the river stage tomography could carry out more information from the measurements and have better resolution in estimating Ks field than the else, at least, in the case of this study. The synthetic experiment also demonstrates that by using aquifer's response to seasonality river stage variation, even though the flood wave migrating from upper to downstream only takes about 8 hours (i.e. the stream stage do not have significant difference along the river), these methods are still a valid technique to identify the basin scale subsurface heterogeneity. This study also reveals that the noise free information carried by hourly basis well and gauge hydrograph records is sufficient enough to evaluate the subsurface characteristics in basin scale at Zhuoshui River alluvial fan. When the geologic zones knowledge is included, the overall estimate improves. However, poor quality prior info will reduce the accuracy of estimated Ks value.

It is found that at Zhuoshui River alluvial fan, the apex of the alluvial fan is region with relative high Ks and is considered as the possible main recharge area of the aquifer. Ks values gradually decrease toward the shoreline of the fan. In addition, Ks at northern alluvial fan is larger than Ks at southern. These findings agree with previous geological surveying.

Knowledge reported in this article is what I have known till now. There are definitely lots of omissions and should be corrected.

10. Reference

Barlow, P. M., L. A. DeSimone, and A. F. Moench (2000), Aquifer response to stream-stage and recharge variations. II. Convolution method and applications, J. Hydrol., 230(3– 4), 211 –229, doi:10.1016/S0022- 1694(00)00176-1.

Bohling, G. C., J. J. Butler Jr., X. Zhan, and M. D. Knoll (2007), A field assessment of the value of steady shape hydraulic tomography for characterization of aquifer heterogeneities, Water Resour. Res., 43, W05430, doi:10.1029/2006WR004932.

Central Geological Survey (1994), The final survey report of the Cho-Shui alluvial fan (in Chinese), Minist. of Econ. Affairs, Taipei, Taiwan.

Central Geological Survey (1999), The hydrogeological survey report of the Cho-Shui alluvial fan (in Chinese), Minist. of Econ. Affairs, Taipei, Taiwan.

Chen, W.P., Lee, C.H., 2003. Estimating ground-water recharge from streamflow records. Environmental Geology 44 (3), 257–265.

Dagan, G. (1982), Stochastic modeling of groundwater flow by unconditional and conditional probabilities. 2. The solute transport, Water Resour. Res., 18(4), 835–848, doi:10.1029/WR018i004p00835.

Davis, E. E., K. Wang, K. Becker, and R. E. Thomson (2000), Formationscale hydraulic and mechanical properties of oceanic crust inferred from pore pressure response to periodic seafloor loading, J. Geophys. Res., 105(B6), 13,423– 13,435, doi:10.1029/2000JB900084.

DeWiest, R. J. M. (1965), Geohydrology, 366 pp., John Wiley, New York.

Duffy, C. J., L. W. Gelhar, and G. W. Gross (1978), Recharge and groundwater conditions in the western region of the Roswell Basin, Rep. 100, N. M. Water Resour. Res. Inst., Las Cruces, N. M.

Hao, Y., T.-C. J. Yeh, J. Xiang, W. A. Illman, K. Ando, and K.-C. Hsu (2008), Hydraulic tomography for detecting fracture connectivity, Ground Water, 46(2), 183– 192, doi:10.1111/j.1745-6584.2007.00388.x.

Henderson, F. M. (1989), Open Channel Flow, 522 pp., MacMillan, New York.

Hoeksema, R. J., and P. K. Kitanidis (1984), An application of the geostatistical approach to the inverse problem in two-dimensional groundwater modeling, Water Resour. Res., 20(7), 1003–1020, doi:10.1029/ WR020i007p01003.

Hsieh, P. A., J. D. Bredehoeft, and S. A. Rojstaczer (1988), Response of well aquifer systems to Earth tides: Problem revisited, Water Resour. Res., 24(3), 468–472, doi:10.1029/WR024i003p00468.

Hughson, D. L., and T.-C. J. Yeh (2000), An inverse model for three-dimensional flow in variably saturated porous media, Water Resour. Res., 36(4), 829–839.

Illman, W. A., X. Liu, and A. Craig (2007), Steady-state hydraulic tomography in a laboratory aquifer with deterministic heterogeneity: Multimethod and multiscale validation of K tomograms, J. Hydrol., 341(3–4), 222– 234, doi:10.1016/j.jhydrol.2007.05.011.

Illman, W. A., X. Liu, S. Takeuchi, T.-C. J. Yeh, K. Ando, and H. Saegusa (2009), Hydraulic tomography in fractured granite: Mizunami Underground Research site, Japan, Water Resour. Res., 45, W01406, doi:10.1029/2007WR006715.

Jang, C.S., Liu, C.W., 2004. Geostatistical analysis and conditional simulation for estimating the spatial variability of hydraulic conductivity in the Choushui River alluvial fan, Taiwan. Hydrological Processes 18 (7), 1333–1350.

Kristopher L. Kuhlman, Andrew C. Hinnell, Phoolendra K. Mishra, Tian-Chyi Jim Yeh (2008) Basin-Scale Transmissivity and Storativity Estimation Using Hydraulic Tomography, Groundwater Volume 46, Issue 5 Pages 706–715

Kitanidis, P. K., and E. G. Vomvoris (1983), A geostatistical approach to the inverse problem in groundwater modeling (steady state) and onedimensional simulations, Water Resour. Res., 19(3), 677–690, doi:10.1029/WR019i003p00677.

Kitanidis, P. K. (1995), Quasi-linear geostatistical theory for inversing, Water Resour. Res., 31(10), 2411–2419, doi:10.1029/95WR01945

Li, B., and T.-C. J. Yeh (1998), Sensitivity and moment analyses of head in variably

saturated regimes, Adv. Water Res., 21(6), 477–485, doi:10.1016/s0309–1708(97)00011-0.

Li, B., and T.-C. J. Yeh (1999), Cokriging estimation of the conductivity field under variably saturated flow conditions, Water Resour. Res., 35(12), 3663–3674, doi:10.1029/1999WR900268.

Li, W., A. Englert, O. A. Cirpka, J. Vanderborght, and H. Vereecken (2007a), Two-dimensional characterization of hydraulic heterogeneity by multiple pumping tests, Water Resour. Res., 43, W04433, doi:10.1029/ 2006WR005333.

Li, H., G. Li, J. Cheng, and M. C. Boufadel (2007b), Tide-induced head fluctuations in a confined aquifer with sediment covering its outlet at the sea floor, Water Resour. Res., 43, W03404, doi:10.1029/2005WR004724.

Lin, Y.-B., Y.-C. Tan, T.-C. J. Yeh, C.-W. Liu, and C.-H. Chen (2004), A viscoelastic model for groundwater level changes in the Cho-Shui River alluvial fan after the Chi-Chi earthquake in Taiwan, Water Resour. Res., 40, W04213, doi:10.1029/2003WR002412.

Liu, S., T.-C. J. Yeh, and R. Gardiner (2002), Effectiveness of hydraulic tomography: Sandbox experiments, Water Resour. Res., 38(4), 1034, doi:10.1029/2001WR000338.

Liu, X., W. A. Illman, A. J. Craig, J. Zhu, and T.-C. J. Yeh (2007), Laboratory sandbox validation of transient hydraulic tomography, Water Resour. Res., 43, W05404, doi:10.1029/2006WR005144.

Lu, Z., and V. V. Vesselinov (2015), Analytical sensitivity analysis of transient groundwater flow in a bounded model domain using the adjoint method, Water Resour. Res., 51, doi:10.1002/2014WR016819.

Mao, D., T.-C. J. Yeh, L. Wan, C.-H. Lee, K.-C. Hsu, J.-C. Wen, and W. Lu (2013), Cross-correlation analysis and information content of observed heads during pumping in unconfined aquifers, Water Resour. Res., 49, doi:10.1002/wrcr.20066.

Nevulis, R. H., D. R. Davis, and S. Sorooshian (1989), Analysis of natural groundwater level variations for hydrogeologic conceptualization, Hanford site, Washington, Water Resour. Res., 25(7), 1519 – 1529,

doi:10.1029/WR025i007p01519.

Rojstaczer, S. (1988), Determination of fluid flow properties from the response of water levels in wells to atmospheric loading, Water Resour. Res., 24(11), 1927–1938, doi:10.1029/WR024i011p01927.

Rojstaczer, S., and F. S. Riley (1990), Response of the water level in a well to Earth tides and atmospheric loading under unconfined conditions, Water Resour. Res., 26(8), 1803–1817.

Straface, S., T.-C. J. Yeh, J. Zhu, S. Troisi, and C. H. Lee (2007), Sequential aquifer tests at a well field, Montalto Uffugo Scalo, Italy, Water Resour. Res., 43, W07432, doi:10.1029/2006WR005287.

Sophocleous, M. A. (1991), Stream-floodwave propagation through the Great Bend alluvial aquifer, Kansas: Field measurements and numerical simulations, J. Hydrol., 124, 207 – 228, doi:10.1016/0022-1694(91) 90015-A.

Sun, R., T.-C. J. Yeh, D. Mao, M. Jin, W. Lu, and Y. Hao (2013), A temporal sampling strategy for hydraulic tomography analysis, Water Resour. Res., 49, 3881–3896, doi:10.1002/wrcr.20337.

Tso, C.-H. M., Y. Zha, T.-C. J. Yeh, and J.-C. Wen (2015), The relative importance of head, flux, and prior information in hydraulic tomography
analysis, Water Resour. Res., 51, doi:10.1002/2015WR017191.

Vazquez-Sune, E., B. Capino, E. Abarca, and J. Carrera (2007), Estimation of recharge from floods in disconnected stream-aquifer systems, Ground Water, 45(5), 579–589, doi:10.1111/j.1745-6584.2007.00326.x.

Vesselinov, V. V., S. P. Neuman, andW. A. Illman (2001), Three-dimensional numerical inversion of pneumatic cross-hole tests in unsaturated fractured tuff: 2. Equivalent parameters, high-resolution stochastic imaging and scale effects, Water Resour. Res., 37(12), 3019 – 3042, doi:10.1029/ 2000WR000135.

Water Resources Agency (2014), Planning groundwater recharge with coupled numerical models of surface and subsurface water (in Chinese), Minist. of Econ. Affairs, Taipei, Taiwan.

Xiang, J., T.-C. J. Yeh, C.-H. Lee, K.-C. Hsu, and J.-C. Wen (2009), A simultaneous successive linear estimator and a guide for hydraulic tomography analysis, Water Resour. Res., 45, W02432, doi:10.1029/2008WR007180.

Yeh, T.-C. J., A. L. Gutjahr, and M. Jin (1995), An iterative cokriging-like technique for ground-water flow modeling, Ground Water, 33(1), 33–41.

Yeh, T.-C. J., M. Jin, and S. Hanna (1996), An Iterative Stochastic Inverse Method: Conditional Effective Transmissivity and Hydraulic Head Fields, Water Resour. Res., 32(1), 85–92, doi:10.1029/95WR02869.

Yeh, T.-C. J., and J. Zhang (1996), A geostatistical inverse method for variably saturated flow in the vadose zone, Water Resour. Res., 32(9), 2757–2766.

Yeh, T.-C. J., and S. Liu (2000), Hydraulic tomography: Development of a new aquifer test method, Water Resour. Res., 36(8), 2095 – 2105, doi:10.1029/2000WR900114.

Yeh, T.-C. J., S. Liu, R. J. Glass, K. Baker, J. R. Brainard, D. Alumbaugh, and D. LaBrecque (2002), A geostatistically based inverse model for electrical resistivity surveys and its applications to vadose zone hydrology, Water Resour. Res., 38(12), 1278, doi:10.1029/2001WR001204.

Yeh, T.-C. J., J. Zhu, A. Englert, A. Guzman, and S. Flaherty (2006), A successive linear estimator for electrical resistivity tomography, in Applied Hydrogeophysics, edited by H. Vereecken et al., pp. 45–74, Springer, Dordrecht, Netherlands.

Yeh, T.-C. J., and J. Zhu (2007), Hydraulic/partitioning tracer tomography for characterization of dense nonaqueous phase liquid source zones, Water Resour. Res., 43, W06435, doi:10.1029/2006WR004877.

Yeh, T.-C. J., J. Xiang, R. M. Suribhatla, K.-C. Hsu, C.-H. Lee, and J.-C. Wen (2009), River stage tomography: A new approach for characterizing groundwater basins, Water Resour. Res., 45, W05409, doi:10.1029/2008WR007233.

Yeh, T.-C. J., Raziuddin Khaleel, and Kenneth C. Carroll (2015), Flow through Heterogeneous Geologic Media, Cambridge Press, ISBN: 9781107076136

Yuanyuan Zha, Tian-Chyi J. Yeh, Deqiang Maob, Jinzhong Yanga, Wenxi Lu (2014), Usefulness of flux measurements during hydraulic tomographic survey for mapping hydraulic conductivity distribution in a fractured medium, Advanced in Water Resources, 71, 162-176

Yuanyuan Zha, Tian-Chyi J. Yeh, Walter A. Illman, Tatsuya Tanaka, Patrick Bruines, Hironori Onoe, Hiromitsu Saegusa (2015), What does hydraulic tomography tell us about fractured geological media? A field study and synthetic experiments, Journal of Hydrology, 531, 17–30

Zhang, J., and T.-C. J. Yeh (1997), An iterative geostatistical inverse method for steady flow, Water Resour. Res., 33

Zhu, J., and T.-C. J. Yeh (2005), Characterization of aquifer heterogeneity using transient hydraulic tomography, Water Resour. Res., 41, W07028, doi:10.1029/2004WR003790.

Zhu, J., and T.-C. J. Yeh (2006), Analysis of hydraulic tomography using temporal moments of drawdown recovery data, Water Resour. Res., 42, W02403, doi:10.1029/2005WR004309.